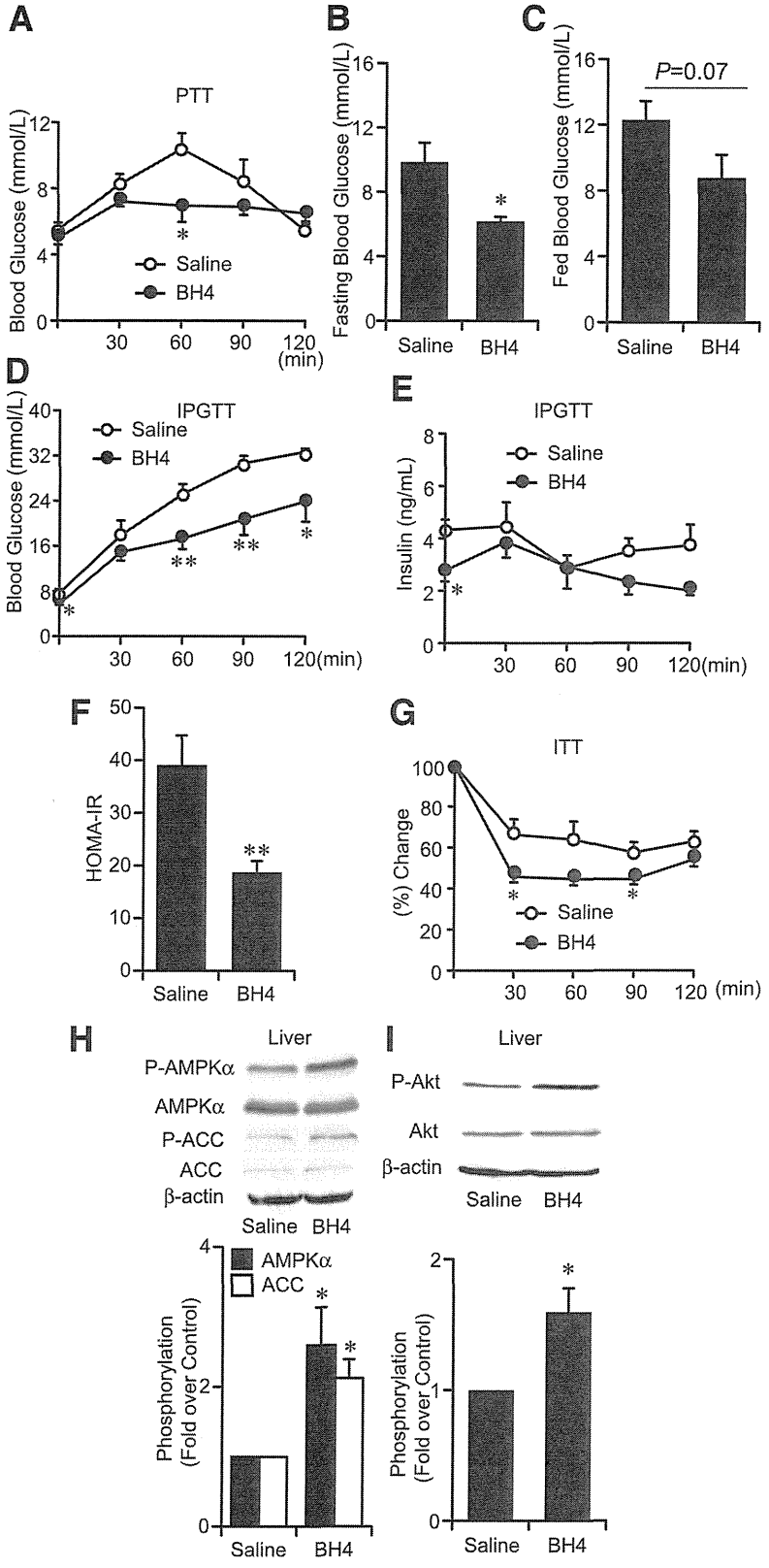

FIG. 7. Effects of BH_4 in *ob/ob* mice. *A*: PTT to *ob/ob* mice with or without single administration of BH_4 (20 mg/kg). Values are means ± SE (n = 6). *P < 0.05 vs. the value of saline. *B*: Fasting blood glucose levels of *ob/ob* mice treated with BH_4 (20 mg/kg/day) for 10 days were significantly decreased compared with those treated without BH_4. Values are means ± SE (n = 6). *P < 0.05 vs. the value of saline. *C*: Fed blood glucose levels in *ob/ob* mice treated with or without BH_4 for 10 days. P = 0.07 vs. the value of saline. Values are means ± SE (n = 6). *D* and *E*: IPGTT to *ob/ob* mice. Blood glucose levels and plasma insulin levels after administration of glucose (1 g/kg i.p.) with or without BH_4 for 10 days. Values are means ± SE (n = 6). *P < 0.05, **P < 0.01 vs. without BH_4. *F*: HOMA-IR calculated from fasting blood glucose and insulin levels from IPGTT data in *ob/ob* mice treated with or without BH_4 for 10 days. Values are means ± SE (n = 6). **P < 0.01 vs. the value of saline. *G*: Insulin tolerance test (ITT) to *ob/ob* mice treated with or without BH_4 for 10 days. Values are means ± SE (n = 6). *P < 0.05 vs. the value of saline. *H* and *I*: AMPKα, ACC, and Akt phosphorylation in liver tissues of *ob/ob* mice was increased by 10 days' administration of BH_4. Data are expressed as fold stimulation over saline. Values are means ± SE (n = 3). *P < 0.05 vs. saline.

The glucose-lowering effect of BH_4 by single administration intraperitoneally on fasting blood glucose levels in STZ diabetic mice was similar to that of metformin (250 mg/kg). The dose of metformin that we used was adjusted to previous studies in mice (43) and is more than fivefold higher than that in clinical use for type 2 diabetic patients (44). We demonstrate here the lowering effects of BH_4 on blood glucose levels using a dosage similar to that of BH_4 used in patients with phenylketonuria as a cofactor of phenylalanine hydroxylase (45).

Numerous clinical trials have been performed on the effect of BH_4 as a cofactor of eNOS on endothelial dysfunction in a variety of vascular diseases including coronary artery disease (15). While many of the results are disappointing (46), BH_4 remains a viable candidate for clinical use if the design of the various trials is reconsidered. Several of the studies reported that BH_4 levels are plainly decreased and that uncoupled eNOS is found in the diabetic state and not in nondiabetic states (47). Moreover, nondiabetic patients were included in most of the clinical trials (46); those trials should be performed in patients with diabetes. The current study, furthermore, clarifies a novel concept of the relationship between BH_4 and glucose metabolism and insulin resistance that suggests a new approach to the prevention of macrovascular complications of diabetes induced by endothelial dysfunction as well as amelioration of the disease itself.

In conclusion, BH_4 has a glucose-lowering effect by suppressing hepatic gluconeogenesis in an eNOS-dependent manner and ameliorates glucose intolerance as well as insulin resistance in diabetic mice, suggesting that BH_4 has potential in the treatment of type 2 diabetes.

ACKNOWLEDGMENTS

This study was supported by Scientific Research grants; a grant for Leading Project for Biosimulation from the Ministry of Education, Culture, Sports, Science, and Technology of Japan; a grant from Core Research for Evolutional Science and Technology (CREST) of Japan Science and Technology Cooperation; a grant from the Ministry of Health, Labor, and Welfare, Japan; and a grant from Kyoto University Global Center of Excellence (COE) Program "Center for Frontier Medicine."

No potential conflicts of interest relevant to this article were reported.

A.A. and Y.F. researched data, contributed to discussion, and wrote, reviewed, and edited the manuscript. A.Ob. and A.Oh. researched data and contributed to discussion. T.F., Y.S., M.O., Y.N., S.F., and M.H. contributed to discussion. H.H. researched data and contributed to discussion. N.I. contributed to discussion and wrote, reviewed, and edited the manuscript. N.I. is the guarantor of this work and, as such, had full access to all the data in the study and takes responsibility for the integrity of the data and the accuracy of the data analysis.

Parts of this study were presented in abstract form at the 71st Scientific Sessions of the American Diabetes Association, San Diego, California, 24–28 June 2011.

The authors thank Ryo Tanaka and Miho Nishimura for their efforts in collaboration in the Student Research Program, Department of Biosciences, Teikyo University of Science and Technology.

REFERENCES

1. Triggle CR, Ding H. A review of endothelial dysfunction in diabetes: a focus on the contribution of a dysfunctional eNOS. J Am Soc Hypertens 2010;4:102–115
2. Huang PL. eNOS, metabolic syndrome and cardiovascular disease. Trends Endocrinol Metab 2009;20:295–302
3. Kim JA, Montagnani M, Koh KK, Quon MJ. Reciprocal relationships between insulin resistance and endothelial dysfunction: molecular and pathophysiological mechanisms. Circulation 2006;113:1888–1904
4. Duplain H, Burcelin R, Sartori C, et al. Insulin resistance, hyperlipidemia, and hypertension in mice lacking endothelial nitric oxide synthase. Circulation 2001;104:342–345
5. Shankar RR, Wu Y, Shen HQ, et al. Mice with gene disruption of both endothelial and neuronal nitric oxide synthase exhibit insulin resistance. Diabetes 2000;49:684–687
6. Stuehr D, Pou S, Rosen GM. Oxygen reduction by nitric-oxide synthases. J Biol Chem 2001;276:14533–14536
7. Vásquez-Vivar J, Kalyanaraman B, Martásek P, et al. Superoxide generation by endothelial nitric oxide synthase: the influence of cofactors. Proc Natl Acad Sci USA 1998;95:9220–9225
8. Crabtree MJ, Channon KM. Synthesis and recycling of tetrahydrobiopterin in endothelial function and vascular disease. Nitric Oxide 2011;25:81–88
9. Landmesser U, Dikalov S, Price SR, et al. Oxidation of tetrahydrobiopterin leads to uncoupling of endothelial cell nitric oxide synthase in hypertension. J Clin Invest 2003;111:1201–1209
10. Meininger CJ, Marinos RS, Hatakeyama K, et al. Impaired nitric oxide production in coronary endothelial cells of the spontaneously diabetic BB rat is due to tetrahydrobiopterin deficiency. Biochem J 2000;349:353–356
11. Xu J, Wu Y, Song P, et al. Proteasome-dependent degradation of guanosine 5′-triphosphate cyclohydrolase I causes tetrahydrobiopterin deficiency in diabetes mellitus. Circulation 2007;116:944–953
12. Meininger CJ, Cai S, Parker JL, et al. GTP cyclohydrolase I gene transfer reverses tetrahydrobiopterin deficiency and increases nitric oxide synthesis in endothelial cells and isolated vessels from diabetic rats. FASEB J 2004;18:1900–1902
13. Ding QF, Hayashi T, Packiasamy AR, et al. The effect of high glucose on NO and O2- through endothelial GTPCH1 and NADPH oxidase. Life Sci 2004;75:3185–3194
14. Kietadisorn R, Juni RP, Moens AL. Tackling endothelial dysfunction by modulating NOS uncoupling: new insights into its pathogenesis and therapeutic possibilities. Am J Physiol Endocrinol Metab 2012;302:E481–E495
15. Katusic ZS, d'Uscio LV, Nath KA. Vascular protection by tetrahydrobiopterin: progress and therapeutic prospects. Trends Pharmacol Sci 2009;30:48–54
16. Wajngot A, Chandramouli V, Schumann WC, et al. Quantitative contributions of gluconeogenesis to glucose production during fasting in type 2 diabetes mellitus. Metabolism 2001;50:47–52
17. Lin HV, Accili D. Hormonal regulation of hepatic glucose production in health and disease. Cell Metab 2011;14:9–19
18. Oyadomari S, Koizumi A, Takeda K, et al. Targeted disruption of the Chop gene delays endoplasmic reticulum stress-mediated diabetes. J Clin Invest 2002;109:525–532
19. Fujita Y, Hosokawa M, Fujimoto S, et al. Metformin suppresses hepatic gluconeogenesis and lowers fasting blood glucose levels through reactive nitrogen species in mice. Diabetologia 2010;53:1472–1481
20. Fujimoto S, Mukai E, Hamamoto Y, et al. Prior exposure to high glucose augments depolarization-induced insulin release by mitigating the decline of ATP level in rat islets. Endocrinology 2002;143:213–221
21. Ogura M, Nakamura Y, Tanaka D, et al. Overexpression of SIRT5 confirms its involvement in deacetylation and activation of carbamoyl phosphate synthetase 1. Biochem Biophys Res Commun 2010;393:73–78
22. Sawabe K, Wakasugi KO, Hasegawa H. Tetrahydrobiopterin uptake in supplemental administration: elevation of tissue tetrahydrobiopterin in mice following uptake of the exogenously oxidized product 7,8-dihydrobiopterin and subsequent reduction by an anti-folate-sensitive process. J Pharmacol Sci 2004;96:124–133
23. Sawabe K, Suetake Y, Nakanishi N, et al. Cellular accumulation of tetrahydrobiopterin following its administration is mediated by two different processes; direct uptake and indirect uptake mediated by a methotrexate-sensitive process. Mol Genet Metab 2005;86(Suppl. 1):S133–S138
24. Hoshiga M, Hatakeyama K, Watanabe M, et al. Autoradiographic distribution of [^{14}C]tetrahydrobiopterin and its developmental change in mice. J Pharmacol Exp Ther 1993;267:971–978
25. Matei V, Rodríguez-Vilarrupla A, Deulofeu R, et al. Three-day tetrahydrobiopterin therapy increases in vivo hepatic NOS activity and reduces portal pressure in CCl4 cirrhotic rats. J Hepatol 2008;49:192–197

26. Elrod JW, Duranski MR, Langston W, et al. eNOS gene therapy exacerbates hepatic ischemia-reperfusion injury in diabetes: a role for eNOS uncoupling. Circ Res 2006;99:78–85
27. Shah V, Cao S, Hendrickson H, et al. Regulation of hepatic eNOS by caveolin and calmodulin after bile duct ligation in rats. Am J Physiol Gastrointest Liver Physiol 2001;280:G1209–G1216
28. Wei CL, Khoo HE, Lee KH, et al. Differential expression and localization of nitric oxide synthases in cirrhotic livers of bile duct-ligated rats. Nitric Oxide 2002;7:91–102
29. McNaughton L, Puttagunta L, Martinez-Cuesta MA, et al. Distribution of nitric oxide synthase in normal and cirrhotic human liver. Proc Natl Acad Sci USA 2002;99:17161–17166
30. Mei Y, Thevananther S. Endothelial nitric oxide synthase is a key mediator of hepatocyte proliferation in response to partial hepatectomy in mice. Hepatology 2011;54:1777–1789
31. Zhang BB, Zhou G, Li C. AMPK: an emerging drug target for diabetes and the metabolic syndrome. Cell Metab 2009;9:407–416
32. Hardie DG. The AMP-activated protein kinase pathway—new players upstream and downstream. J Cell Sci 2004;117:5479–5487
33. Carabaza A, Ricart MD, Mor A, et al. Role of AMP on the activation of glycogen synthase and phosphorylase by adenosine, fructose, and glutamine in rat hepatocytes. J Biol Chem 1990;265:2724–2732
34. Ouyang J, Parakhia RA, Ochs RS. Metformin activates AMP kinase through inhibition of AMP deaminase. J Biol Chem 2011;286:1–11
35. Fogarty S, Hardie DG. Development of protein kinase activators: AMPK as a target in metabolic disorders and cancer. Biochim Biophys Acta 2010; 1804:581–589
36. Kojima S, Ona S, Iizuka I, et al. Antioxidative activity of 5,6,7,8-tetrahydrobiopterin and its inhibitory effect on paraquat-induced cell toxicity in cultured rat hepatocytes. Free Radic Res 1995;23:419–430
37. Delgado-Esteban M, Almeida A, Medina JM. Tetrahydrobiopterin deficiency increases neuronal vulnerability to hypoxia. J Neurochem 2002;82:1148–1159
38. Kang KT, Sullivan JC, Spradley FT, et al. Antihypertensive therapy increases tetrahydrobiopterin levels and NO/cGMP signaling in small arteries of angiotensin II-infused hypertensive rats. Am J Physiol Heart Circ Physiol 2011;300:H718–H724
39. Higaki Y, Hirshman MF, Fujii N, et al. Nitric oxide increases glucose uptake through a mechanism that is distinct from the insulin and contraction pathways in rat skeletal muscle. Diabetes 2001;50:241–247
40. Zhang J, Xie Z, Dong Y, et al. Identification of nitric oxide as an endogenous activator of the AMP-activated protein kinase in vascular endothelial cells. J Biol Chem 2008;283:27452–27461
41. Viollet B, Guigas B, Leclerc J, et al. AMP-activated protein kinase in the regulation of hepatic energy metabolism: from physiology to therapeutic perspectives. Acta Physiol (Oxf) 2009;196:81–98
42. Cook S, Scherrer U. Insulin resistance, a new target for nitric oxide-delivery drugs. Fundam Clin Pharmacol 2002;16:441–453
43. Shaw RJ, Lamia KA, Vasquez D, et al. The kinase LKB1 mediates glucose homeostasis in liver and therapeutic effects of metformin. Science 2005; 310:1642–1646
44. Inzucchi SE, Maggs DG, Spollett GR, et al. Efficacy and metabolic effects of metformin and troglitazone in type II diabetes mellitus. N Engl J Med 1998;338:867–872
45. Blau N. Defining tetrahydrobiopterin (BH4)-responsiveness in PKU. J Inherit Metab Dis 2008;31:2–3
46. Moens AL, Kietadisorn R, Lin JY, et al. Targeting endothelial and myocardial dysfunction with tetrahydrobiopterin. J Mol Cell Cardiol 2011;51:559–563
47. Heitzer T, Krohn K, Albers S, et al. Tetrahydrobiopterin improves endothelium-dependent vasodilation by increasing nitric oxide activity in patients with Type II diabetes mellitus. Diabetologia 2000;43:1435–1438

FEBS Letters 586 (2012) 4076–4081

journal homepage: www.FEBSLetters.org

SIRT5 deacetylates and activates urate oxidase in liver mitochondria of mice

Yasuhiko Nakamura, Masahito Ogura, Kasane Ogura, Daisuke Tanaka, Nobuya Inagaki *

Department of Diabetes and Clinical Nutrition, Graduate School of Medicine, Kyoto University, Kyoto 606-8507, Japan

ARTICLE INFO

Article history:
Received 16 August 2012
Revised 26 September 2012
Accepted 4 October 2012
Available online 16 October 2012

Edited by Vladimir Skulachev

Keywords:
SIRT5
Urate oxidase
Mouse
Liver
Mitochondria

ABSTRACT

We identified urate oxidase (UOX) as a target of SIRT5 by comparing mitochondrial proteins in livers of SIRT5-overexpressing transgenic (SIRT5 Tg) and wild-type mice by using two-dimensional electrophoresis. Acetylation levels of UOX in liver of SIRT5 Tg mice were approximately half of those in wild-type mice, and UOX activity was significantly increased. *In vitro*-synthesized UOX protein was acetylated when incubated with mitochondria from wild-type mice liver but the levels were less when incubated with those from SIRT5 Tg mice liver. These results suggest that SIRT5 activates UOX through deacetylation in mouse liver mitochondria.

Structured summary of protein interactions:
Uox physically interacts with **Sirt5** by anti bait coimmunoprecipitation (View interaction)
Catalase, **Hsp60** and **Uox** colocalize by cosedimentation through density gradient (View interaction)
Hsp60, **Uox** and **Sirt5** colocalize by cosedimentation through density gradient (View interaction)

1. Introduction

It is known that lifespan is prolonged by calorie restriction in species ranging from yeast to mice [1–3]. Recently, a 20-year longitudinal study in monkeys revealed that calorie restriction suppressed risk of development of age-associated disease involving brain atrophy, neoplasia, cardiovascular disease, and glucoregulatory impairment, thereby diminishing the incidence of age-dependent death [4]. It is also reported that disruption of SIR2, which is a NAD^+-dependent histone deacetylase in nucleus, abolishes lifespan extension by calorie restriction in yeast [5]. Mammals have seven SIR2 homologues in the SIRT family (SIRT1–7). Among them, SIRT1, SIRT2, SIRT3, and SIRT5 have NAD^+-dependent protein deacetylase activity. [6]. It is thought that SIRTs recognize the decrease in energy levels of the cell by calorie restriction as an increase in NAD^+ content [7]. SIRT5 protein, a member of the SIRT family, is known to locate in mitochondria [8–10], and has not only the NAD^+-dependent deacetylase activity but also NAD^+-dependent desuccinylase and demalonylase activities [6,11]. Recently, we [12] and the Guarente group [13] found independently that carbamoyl phosphate synthase 1 (CPS1) is a SIRT5 substrate protein by using SIRT5-overexpressing transgenic (SIRT5 Tg) mice and SIRT5 knock-out mice, respectively. CPS1 is a key enzyme in the urea cycle, which detoxifies ammonia generated in liver as a by-product of gluconeogenesis from amino acids during fasting and starvation. Ammonia is finally converted to urea in liver and is excreted from kidney. We demonstrate that SIRT5 mRNA levels are increased and that CPS1 protein is deacetylated and activated by SIRT5 during fasting in mouse liver [14]. SIRT5 also deacetylates cytochrome c [10], but its role is still unknown.

Urate oxidase (UOX) is a crucial enzyme that catalyzes conversion of urate to allantoin, which has higher water solubility than urate, the last step of purine catabolism in most mammals [14] except human and hominoid primates including chimpanzee, gorilla, and orangutan, which lack UOX activity [15]. In the present study, to clarify the novel function and physiological role of SIRT5 protein in liver of mice, we attempted to identify a novel protein that is deacetylated and regulated by SIRT5 using SIRT5 Tg mice. We demonstrate here that SIRT5 may regulate purine catabolism through deacetylation and activation of UOX protein.

2. Materials and methods

Animal experiments: The mice were housed in an air-controlled (temperature 25 °C) room with dark-light cycle (10; 14 h). Animal care and procedures were approved by the Animal Care Committee of Kyoto University. As both lines (#36, #38) of 8–12 week-old SIRT5-overexpressing transgenic (SIRT5 Tg) mice showed similar data, all experiments were performed using one line (#36) and its littermate wild-type mice [12].

Abbreviations: UOX, urate oxidase; SIRT5 Tg, SIRT5-overexpressing transgenic; CPS1, carbamoyl phosphate synthetase 1

* Corresponding author. Address: Department of Diabetes and Clinical Nutrition, Graduate School of Medicine, Kyoto University, 54 Kawahara-cho, Shogoin, Sakyo-ku, Kyoto 606 8507, Japan. Fax: +81 75 771 6601.
E-mail address: inagaki@metab.kuhp.kyoto-u.ac.jp (N. Inagaki).

0014-5793/$36.00 © 2012 Federation of European Biochemical Societies. Published by Elsevier B.V. All rights reserved.
http://dx.doi.org/10.1016/j.febslet.2012.10.009

Preparation of 10 k fraction and cytosol: Preparation of mitochondria particle-enriched 10 k fraction from liver was performed as described previously [16]. Liver from mice was disrupted in isotonic buffer (PBS containing 0.2 M mannitol, 0.07 M sucrose, and 1 mM EDTA) with potter homogenizer, followed by centrifugation at 800*g* at 4 °C for 10 min to obtain post-nuclear supernatant. Post-nuclear supernatant was centrifuged at 10,000*g* at 4 °C for 10 min to obtain the mitochondria particle-enriched precipitate and post-mitochondria supernatant. The precipitate was suspended with isotonic buffer and the 10 k fraction was obtained. Post-mitochondria supernatant was then ultracentrifuged at 100,000*g* at 4 °C for 30 min, and cytosol was obtained as a supernatant.

Separation of 10 k fraction into purified mitochondria and peroxisomes: Self-generated density gradient method with OptiPrep (COSMO BIO) was performed for separation of 10 k fractions. The fraction was suspended in 6 ml 25 % OptiPrep containing 60 mM Mops-NaOH buffer (pH7.4), 0.25 M sucrose, 1 mM EDTA, and 0.1 % (v/v) ethanol. The suspension was centrifuged at 180,000*g* at 4 °C for 3 h in a fixed-angle rotor. The fractions were collected from the density gradient by 500 μL of each upward displacement.

Two-dimensional electrophoresis and identification of protein: the 10 k fraction was lysed with rehydration buffer (8 M urea, 2% CHAPS, 50 mM DTT, 0.2% Bio-Lyte (BIO-RAD), 0.001% bromophenol blue), and applied to ReadyStrip IPG Strip (BIO-RAD) and separated by isoelectric focusing electrophoresis with a range pH 7 to pH 10 using PROTEAN IEF cell (BIO-RAD). The IPG Strip was then subjected to SDS–polyacrylamide gel electrophoresis. The obtained gel was immunoblotted using anti-acetylated lysine antibody (Cell Signaling). The acetylated proteins were visualized and analyzed using Las 4000 mini (FUJIFILM). The protein spot the intensity of which was decreased in SIRT5 Tg mice compared to wild-type mice was isolated from another two-dimensional electrophoresed gel and treated with trypsin; the peptides obtained at the indicated spot were analyzed using MALDI-TOF-MS (APRO Life Science Institute, Inc.).

Measurement of urate oxidase activity: 10 k fractions from livers of SIRT5 Tg and wild-type mice were used for determination of urate oxidase. Urate oxidase activity was assayed as described by Priest and Pitts [17]. Briefly, the reaction was started by adding the 10 k fraction to the assay mixture containing 50 mM sodium borate buffer (pH 8.5) and 0.125 mM urate sodium salt at room temperature, and the decrease in absorbance at 292 nm was measured. One unit of urate oxidase activity corresponded to degradation of 1 mmol of urate at room temperature.

Immunoprecipitation: Mitochondria lysed with PBS containing 1 % Triton X-100 were incubated with anti-acetylated lysine antibody for 16 h at 4 °C. Protein G Sepharose (GE healthcare) resin was then added and incubation was continued for 3 h. The resin was washed five times with PBS containing 0.1 % Triton X-100 and boiled with SDS sample buffer (0.2 M Tris, 10% sucrose, 10% SDS, 5 mM EDTA). The sample was analyzed by immunoblotting with anti-UOX (Cell Signaling) or anti-acetylated lysine or anti-myc (Santa Cruz) antibody.

In vitro synthesis of non-acetylated UOX and incubation with mitochondria and/or cytosol: Non-acetylated and myc-tag fused UOX protein was synthesized using PURESYSTEM classic II (BioComber). UOX-myc template DNA for PURESYSTEM classic II was synthesized by PCR using primers "GAAATTAATACGACTCACTATAGGGAGACCACAACGGTTTCCCTCTAGAAATAATTTTGTTTAACTTTAAGAAGGAGATATACCAATGGCCCATTAC", "TATTCATTACAAGTCCTCTTCAGAAATGAGCTTTTGCTCCAGCCTGGAAGGCAGCTTCC", and UOX cDNA as a template. The obtained UOX-myc template DNA was added to solution containing PURESYSTEM solution A, PURESYSTEM solution B, 2 μg/μl purified liver mitochondria from SIRT5 Tg mice or wild-type mice, and/or 2 μg/μl mice liver cytosol, and incubated for 1 h at 37 °C. Obtained solutions were lysed with 1% Triton X-100 and immunoprecipitated using anti-myc antibody and then analyzed by immunoblotting using anti-myc antibody or anti-acetylated lysine antibody.

3. Results

3.1. Identification of UOX as a target of SIRT5 protein

We already established two SIRT5-overexpressing transgenic (SIRT5 Tg) mice lines [10]. We hypothesize that deacetylation of SIRT5 substrate proteins may be promoted in liver of SIRT5 Tg mice compared to that in wild-type mice. To search for a novel substrate protein of SIRT5, we performed two-dimensional electrophoresis and immunoblotting using anti-acetylated lysine antibody. As SIRT5 is expressed in mitochondria, mitochondria-enriched 10 k fractions from livers of SIRT5 Tg and wild-type mice were prepared and subjected to isoelectric focusing electrophoresis, and separated by SDS–PAGE. The acetylated proteins were then observed by immunoblotting with anti-acetylated lysine antibody. One of the proteins with spots having decreased intensity in liver of SIRT5 Tg mice (Fig. 1A, indicated by arrows) was picked up from another electrophoresed two-dimensional gels of 10 k fraction in wild-type mice, treated with trypsin, and analyzed by MALDI-TOF-MS (Fig. 1B). The protein was identified as urate oxidase (UOX) from peptide sequences determined by mass spectrometry (Table 1).

3.2. UOX is located both in mitochondria and peroxisomes

In mice, localization of UOX is controversial; some reports demonstrate that UOX is located in mitochondria [18,19] while others find localization in peroxisomes [20]. In fact, mitochondria-enriched 10 k fraction from liver of wild-type mice contains not only mitochondria but also peroxisomes. Thus, to clarify subcellular distribution of UOX, we performed self-generated density gradient by high-speed ultracentrifugation using OptiPrep to separate mitochondria from peroxisomes.

The 10 k fraction prepared from liver of wild-type mice was suspended by 25% OptiPrep solution, and ultracentrifuged at 180,000*g* at 4 °C. Samples were collected from the obtained density gradient by 500 μL of each upward displacement, and analyzed by immunoblotting using anti-hsp60 antibody as a mitochondrial marker, anti-catalase antibody as a peroxisomes marker, anti-UOX antibody, and anti-SIRT5 antibody (Fig. 2A). Mitochondria were distributed mainly in the top fractions of the density gradient, while peroxisomes were distributed mainly in the bottom fractions. UOX was distributed in both the top and bottom fractions, suggesting that UOX is located both in mitochondria and peroxisomes. To ascertain localization of UOX, we collected the top and bottom three fractions as the purified mitochondria and peroxisomes fractions, respectively, and the purified fractions were subjected to immunoblotting for hsp60, catalase, UOX, and SIRT5 (Fig. 2B). The relative ratio of SIRT5 protein level in mitochondria and peroxisomes fractions was not significantly different from that of hsp60, suggesting that SIRT5 is localized only in mitochondria. The relative ratio of UOX protein level in purified mitochondria fraction was significantly higher than that of contaminated catalase in purified mitochondria fraction, indicating that UOX is located both in peroxisomes and mitochondria.

3.3. UOX is deacetylated and activated in liver mitochondria of SIRT5 Tg mice

To confirm the result of two-dimensional electrophoresis, 10 k fractions from SIRT5 Tg and wild-type mice were lysed by Triton-X 100 and immunoprecipitated using anti-UOX antibody. The

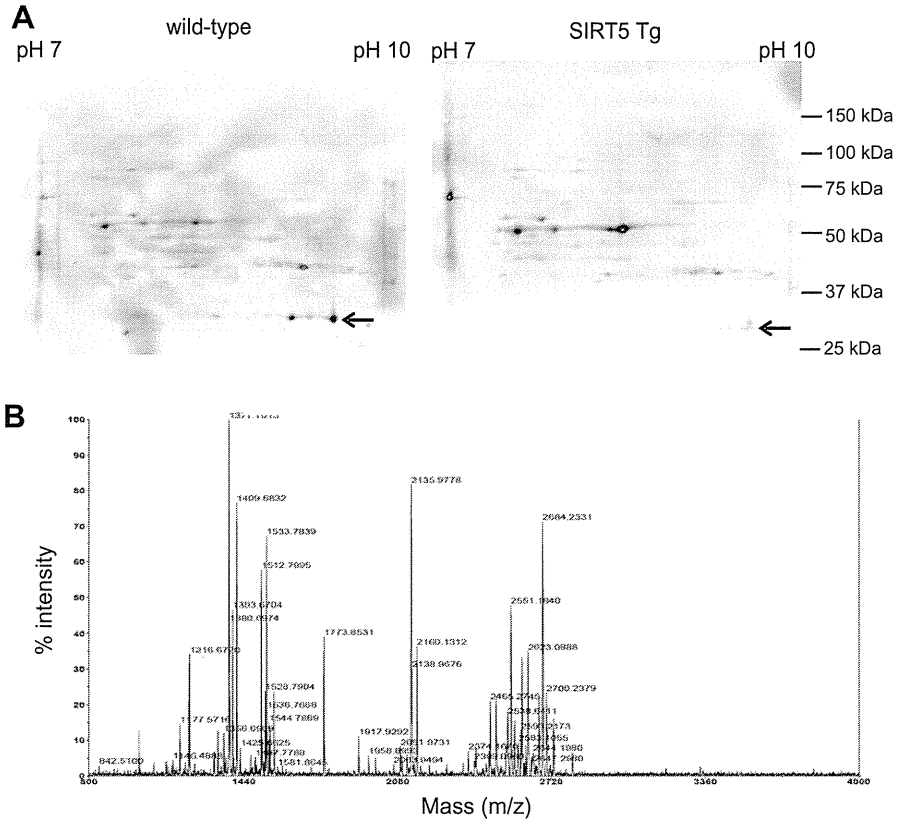

Fig. 1. Identification of the target protein of SIRT5. (A) Immunoblot analyses of two-dimensional electrophoresed gels of the mitochondria-enriched 10 k proteins prepared from livers of SIRT5 Tg and wild-type mice. The acetylated proteins were detected by immunoblotting using anti-acetylated lysine antibody. The position of the mitochondrial protein prepared from wild-type liver identified by MALDI-TOF-MS is shown by arrow (left panel). The acetylation level is decreased at the corresponding position in SIRT5 Tg liver (indicated by arrow, right panel). (B) MALDI-TOF-MS analysis. The mitochondrial protein prepared from wild-type liver indicated in (A) was analyzed using MALDI-TOF-MS.

Table 1
Characterization by MALDI-TOF-MS of the target protein of SIRT5.

Measured peptide mass (Da)	Corresponding UOX peptide sequence	Start-end
1006.4720	NDEVEFVR	11–18
1175.5104	CFATQVYCK	188–196
1215.6823	EVATSVQLTLR	42–52
1376.6725	DVDFEAIWGAVR	203–214
1511.7885	AHVYVEEVPWKR	108–119
1532.7736	RDVDFEAIWGAVR	202–214
1771.8417	FAGPYDKGEYSPSVQK	221–236
1915.9163	DYLHGDNSDIIPTDTIK	56–72
2158.1344	MGLINKEEVLLPLDNPYGK	272–290
2372.1900	TTQSGFEGFLKDQFTTLPEVK	165–185
2549.1693	HVHAFIHTPTGTHFCEVEQMR	127–147
2682.2319	NIETFAMNICEHFLSSFNHVTR	86–107

Mass of peptides corresponding to a tryptic digest of UOX. The corresponding sequence and position (number of amino acid residues) in the sequence are indicated.

obtained precipitates were then analyzed by SDS–PAGE followed by immunoblotting by anti-UOX and anti-acetylated lysine antibodies (Fig. 3A). The expression levels of UOX were not significantly different in SIRT5 Tg and wild-type mice, but the acetylation level of UOX in SIRT5 Tg mice was approximately half of that in wild-type mice (Fig. 3B). Furthermore, activity of UOX was measured using 10 k fraction from liver of SIRT5 Tg and wild-type mice. UOX activity was significantly increased 1.4-fold in SIRT5 Tg mice compared to that in wild-type mice (Fig. 3C). To investigate whether SIRT5 protein directly interacts with UOX protein, we performed co-immunoprecipitation assay (Fig. 3D); 10 k fraction prepared from liver of wild-type mice was lysed by 1% Triton X-100 and immunoprecipitated with or without anti-UOX antibody and Protein G Sepharose resin, and the resin were boiled with SDS sample buffer. The obtained samples were immunoblotted using anti-UOX antibody and anti-SIRT5 antibody. SIRT5 protein precipitate was detected with the precipitation of UOX protein. Therefore it indicates that SIRT5 protein directly interacts with UOX protein.

3.4. UOX is acetylated and deacetylated in liver mitochondria

From the results above, it is likely that UOX protein is deacetylated by SIRT5. However, it remains unclear how UOX is acetylated

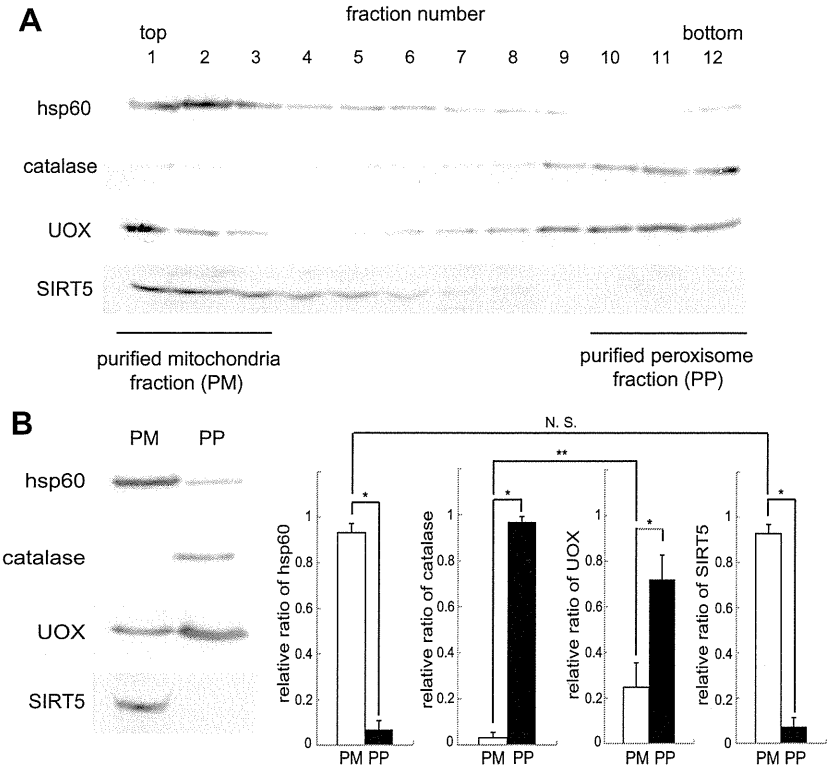

Fig. 2. Determination of UOX subcellular localization. (A) Density gradient of 10 k fraction using OptiPrep. The 10 k fraction was divided into mitochondria and peroxisomes by using self-generated density gradient. Hsp60 and catalase were used as control for mitochondria and peroxisomes, respectively. (B) UOX distribution in purified mitochondria and peroxisomes. Purified mitochondria (PM) and peroxisomes (PP) indicated in Fig. 2A were collected and immunoblotted by using anti-hsp60 (mitochondria marker), anti-catalase (peroxisomes marker), anti-UOX antibodies, and SIRT5 (left panel). Relative expression ratio of these proteins (PM/PM + PP and PP/PM + PP) are calculated by LAS-4000 mini and shown in right panel ($N = 3$). Values are means ± SEM. $^{*}P < 0.01$. $^{**}P < 0.05$. N. S.: no significant difference.

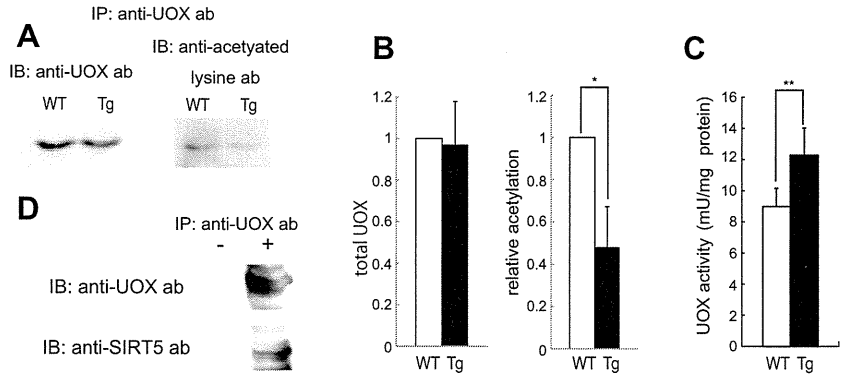

Fig. 3. Deacetylation and activation of UOX in livers of SIRT5 Tg mice. (A) UOX deacetylation in livers of SIRT5 Tg mice. The 10 k fractions from livers of SIRT5 Tg (Tg) and wild-type (WT) mice were immunoprecipitated with anti-UOX antibody, and then immunoblotted with anti-UOX antibody or anti-acetylated lysine antibody. The left two panels show immunoblotting of total UOX protein and acetylated UOX protein in mitochondria. (B) Measurement of acetylation ratio of UOX from wild-type and SIRT5 Tg mice. The ratio of acetylated UOX protein of SIRT5 Tg liver to that of wild-type liver was calculated from densitometry of immunoblotting ($N = 3$; right two panels). (C) Activation of UOX activity in SIRT5 Tg liver. 10 k fractions of livers in SIRT5 Tg ($N = 10$) and wild-type ($N = 10$) mice were used to determine the UOX activities. (D) Interaction between UOX and SIRT5. 10 k fraction was lysed by 1% Triton X-100 and immunoprecipitated with (+) or without (−) anti-UOX antibody. Then immunoblot was performed using anti-UOX antibody or anti-acetylated lysine antibody. Values are means ± SEM. $^{*}P < 0.01$. $^{**}P < 0.05$.

in the cell at physiological condition. We then investigated to find the component of the cell in which UOX protein is acetylated. First, to differentiate in vitro-synthesized UOX from endogenous UOX, UOX protein to which myc-tag was fused at C-terminus (UOX-myc) was synthesized *in vitro* (Fig. 4A). It was confirmed that there was no non-specific protein band in the UOX-myc synthetic solution by immunoblotting using anti-UOX antibody, and that the synthesized UOX protein was not acetylated by immunoblotting using anti-acetylated lysine antibody (Fig. 4A). Next, UOX-myc protein was synthesized with purified mitochondria from SIRT5 Tg mice or wild-type mice and with cytosol. After 1 h incubation, obtained suspensions were lysed by 1% Triton X-100 and immunoprecipitated by anti-myc antibody, followed by immunoblotting using anti-myc or anti-acetylated lysine antibodies (Fig. 4B). Total synthesized UOX-myc protein levels were similar in all samples. However, UOX-myc protein was acetylated only when it was incubated with mitochondria. Furthermore, acetylation levels of UOX protein in the presence of mitochondria from SIRT5 Tg mice were decreased compared to those in the presence of mitochondria from wild-type mice. These results suggest that UOX protein is acety-

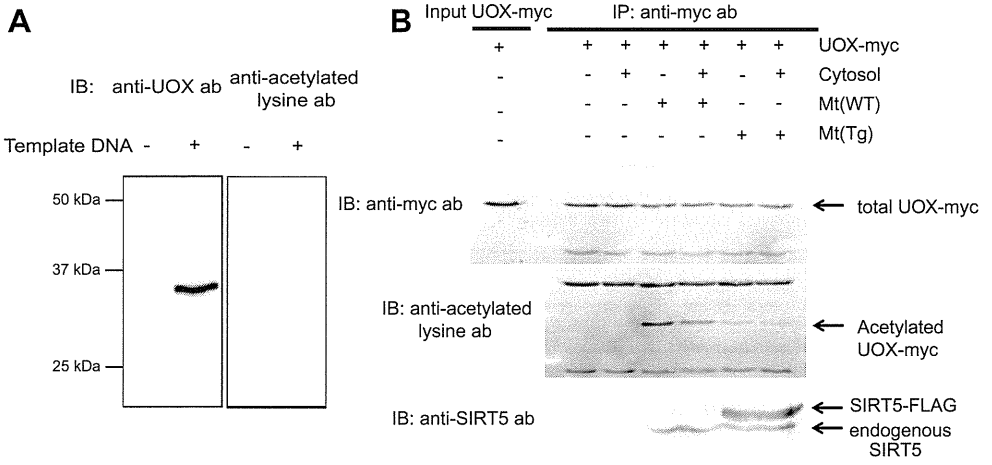

Fig. 4. Acetylation of UOX in mitochondria. (A) *In vitro* synthesis of non-acetylated UOX protein. Non-acetylated UOX-myc was synthesized by using PURESYSTEM classic II with or without UOX-myc template. Synthesized UOX-myc was validated by immunoblotteing using anti-UOX and anti-acetylated lysine antibodies. (B) Incubation of *in vitro*-synthesized UOX-myc with mitochondria. UOX-myc protein was synthesized with mice liver cytosol and/or purified mitochondria from SIRT5 Tg (Mt(Tg))mice or wilt-type (Mt(WT)) mice, and obtained solutions were lysed and immunoprecipitated using anti-myc antibody, followed by immunoblotting using anti-myc antibody (total UOC-myc) or anti-acetylated lysine antibody (acetylated UOX-myc). Mitochondrial endogenous SIRT5 and transgene derived SIRT5-FLAG are indicated in lower panel.

lated in mitochondria and that SIRT5 in mitochondria deacetylates the UOX protein.

4. Discussion

We already reported that SIRT5 mRNA expression level was significantly increased in liver of wild-type mice during fasting compared to that during feeding ad libitum [12], and Guarente group also reported SIRT5 was activated during fasting [13]. Therefore, it is thought that liver of SIRT5-overexpressing transgenic (SIRT5 Tg) mice mimics that of fasting wild-type mice.

In the present study, we attempted to identify a novel mitochondrial protein as the substrate of SIRT5 since SIRT5 is expressed in mitochondria. Mitochondria-enriched 10 k fraction from livers of SIRT5 Tg mice and littermate wild-type mice were analyzed by two-dimensional electrophoresis, immunoblotting using anti-acetylated lysine antibody, and MALDI-TOF-MS. UOX protein was identified as a novel SIRT5 substrate. There are reports showing that UOX protein locates in peroxisomes [20], but we found that UOX protein locates not only in peroxisomes but also in mitochondria using a density gradient method. In addition, our finding that *in vitro*-synthesized UOX-myc protein was acetylated when it was incubated with mitochondria strongly supports UOX localization at mitochondria. Kim et al. reported that UOX has at least 10 potential acetylation sites at lysine residues and that the acetylation state differs during ad libitum feeding and fasting in liver mitochondria [19], suggesting that lysine residue of UOX may be deacetylaed by SIRT5 during fasting.

It has been reported that SIRT5 has not only NAD^+-dependent deacetylase activity but also NAD^+-dependent desuccinylase and demalonylase activities [6,11]. Acetylation levels of UOX protein in SIRT5 Tg mice were clearly decreased compared to those in wild-type mice. However, as anti-acetylated lysine antibodies including the antibody we use here are not fully specific and also recognize differently acylated lysines, the type of UOX acyl modification removed by SIRT5 remains to be confirmed. Furthermore, we could not determine the succinylation and malonylation levels of UOX protein. Therefore, we cannot exclude the possibility that desuccinylation and demalonylation of UOX protein are involved in its activation.

In mice, knock-out of UOX gene leads to hyperuricemia and urate nephropathy and more than half of these mice die before 4 weeks of age [21]. Thus, UOX is a critical protein for survival in mice. Urate is generated in liver by purine body, which is derived mainly from skeletal muscle, and serum urate levels are elevated during fasting and starvation. In the present study, we demonstrated that acetylation levels of UOX in liver of SIRT5 Tg mice were approximately half of those in wild-type mice and that the UOX activity was significantly increased in liver of SIRT5 Tg mice compared to that in wild-type mice. Considered together, our results indicate that mRNA levels of SIRT5 are increased and that UOX protein is deacetylated and activated by SIRT5 during fasting. As we [12] and the Guarente group [13] have reported, SIRT5 regulates the urea cycle by deacetylation and activation of CPS1. SIRT5 has an important role in nitrogen metabolism at fasting and starvation state in mitochondria as both urate and urea are products of nitrogen metabolism from nucleic acid and amino acid, respectively.

To determine the cellular compartment where UOX is acetylated, we incubated in vitro-synthesized, non-acetylated UOX with mitochondria. UOX protein was not acetylated in the presence of cytosol but it was acetylated in the presence of mitochondria. In addition, UOX acetylation levels were lower when incubated with liver mitochondria of SIRT5 Tg mice in comparison with wild-type mice. These results demonstrate that the lysine residue of UOX protein is acetylated in mitochondria in physiological conditions and that there is an acetylation–deacetylation cycle in mitochondria.

In human, the UOX gene is absent. However, recombinant UOX protein is used in treatment as an anti-hyperuricemia agent in tumor lysis syndrome [22–24]. Clarifying the regulatory mechanism of UOX activation by SIRT5 should be useful to develop a more effective agent.

Acknowledgments

This study was supported by Scientific Research Grants from the Ministry of Education, Culture, Sports, Science, and Technology of Japan and from the Ministry of Health, Labor, Welfare, Japan, by a CREST grant from the Japan Science and Technology Agency, and by the Kyoto University Global COE Program "Center for Frontier Medicine".

References

[1] Imai, S., Armstrong, C.M., Kaeberlein, M. and Guarente, L. (2000) Transcriptional silencing and longevity protein Sir2 is an NAD-dependent histone deacetylase. Nature 403, 795–800.

[2] Tissenbaum, H.A. and Guarente, L. (2001) Increased dosage of a sir-2 gene extends lifespan in *Caenorhabditis elegans*. Nature 410, 227–230.
[3] Rogina, B. and Helfand, S.L. (2004) Sir2 mediates longevity in the fly through a pathway related to calorie restriction. Proc. Natl. Acad. Sci. USA 101, 15998–16003.
[4] Colman, R.J., Anderson, R.M., Johnson, S.C., Kastman, E.K., Kosmatka, J.K., Beasley, T.M., Allison, D.B., Cruzen, C., Simmons, H.A., Kemnitz, J.W. and Weindruch, R. (2009) Caloric restriction delays disease onset and mortality in rhesus monkeys. Science 325 (5937), 201–204.
[5] Kaeberlein, M., McVey, M. and Guarente, L. (1999) The SIR2/3/4 complex and SIR2 alone promote longevity in *Saccharomyces cerevisiae* by two different mechanisms. Genes Dev. 13, 2570–2580.
[6] Du, J., Zhou, Y., Su, X., Yu, J.J., Khan, S., Jiang, H., Kim, J., Woo, J., Kim, J.H., Choi, B.H., He, B., Chen, W., Zhang, S., Cerione, R.A., Auwerx, J., Hao, Q. and Lin, H. (2011) Sirt5 is a NAD-dependent protein lysine demalonylase and desuccinylase. Science 334 (6057), 806–809.
[7] Satoh, A., Stein, L. and Imai, S. (2011) The role of mammalian sirtuins in the regulation of metabolism, aging, and longevity. Handb. Exp. Pharmacol. 206, 125–162.
[8] Nakamura, Y., Ogura, M., Tanaka, D. and Inagaki, N. (2008) Localization of mouse mitochondrial SIRT proteins: shift of SIRT3 to nucleus by co-expression with SIRT5. Biochem. Biophys. Res. Commun. 366 (1), 174–179.
[9] Michishita, E., Park, J.Y., Burneskis, J.M., Barrette, J.C. and Horikawa, I. (2005) Evolutionarily conserved and nonconserved cellular localizations and functions of human SIRT proteins. Mol. Biol. Cell 16 (10), 4623–4635.
[10] Schlicker, C., Gertz, M., Papatheodorou, P., Kachholz, B., Becker, C.F. and Steegborn, C. (2008) Substrates and regulation mechanisms for the human mitochondrial sirtuins Sirt3 and Sirt5. J. Mol. Biol. 382 (3), 790–801.
[11] Peng, C., Lu, Z., Xie, Z., Cheng, Z., Chen, Y., Tan, M., Luo, H., Zhang, Y., He, W., Yang, K., Zwaans, B.M., Tishkoff, D., Ho, L., Lombard, D., He, T.C., Dai, J., Verdin, E., Ye, Y. and Zhao, Y. (2011) The first identification of lysine malonylation substrates and its regulatory enzyme. Mol. Cell. Proteomics 10 (12). M111.012658.
[12] Ogura, M., Nakamura, Y., Tanaka, D., Zhuang, X., Fujita, Y., Obara, A., Hamasaki, A., Hosokawa, M. and Inagaki, N. (2010) Overexpression of SIRT5 confirms its involvement in deacetylation and activation of carbamoyl phosphate synthetase 1. Biochem. Biophys. Res. Commun. 393 (1), 73–78.
[13] Nakagawa, T., Lomb, D.J., Haigis, M.C. and Guarente, L. (2009) SIRT5 deacetylates carbamoyl phosphate synthetase 1 and regulates the urea cycle. Cell 137 (3), 560–570.
[14] Álvarez-Lario, B. and Macarrón-Vicente, J. (2010) Uric acid and evolution. Rheumatology 49 (11), 2010–2015.
[15] Wu, X.W., Muzny, D.M., Lee, C.C. and Caskey, C.T. (1992) Two independent mutational events in the loss of urate oxidase during hominoid evolution. J. Mol. Evol. 34 (1), 78–84.
[16] Nakamura, Y., Suzuki, H., Sakaguchi, M. and Mihara, K. (2004) Targeting and assembly of rat mitochondrial translocase of outer membrane 22 (TOM22) into the TOM complex. J. Biol. Chem. 279 (20), 21223–21232.
[17] Priest, D.G. and Pitts, O.M. (1972) Reaction intermediate effects on the spectrophotometric uricase assay. Anal. Biochem. 50 (1), 195–205.
[18] Yokota, S. (1973) Studies on mouse liver urate oxidase II. Immunochemical and enzymatic distribution of urate oxidase in mouse liver cell fractions. Histochemie 37, 149–159.
[19] Kim, S.C., Sprung, R., Chen, Y., Xu, Y., Ball, H., Pei, J., Cheng, T., Kho, Y., Xiao, H., Xiao, L., Grishin, N.V., White, M., Yang, X.J. and Zhao, Y. (2006) Substrate and functional diversity of lysine acetylation revealed by a proteomics survey. Mol. Cell 23 (4), 607–618.
[20] Yeldandi, A.V., Chu, R., Pan, J., Zhu, Y. and Usuda, Y. (1996) Peroxisomal purine metabolism. Ann. N. Y. Acad. Sci. 804, 165–175.
[21] Wu, X., Wakamiya, M., Vaishnav, S., Geske, R., Montgomery, C., Jones, P., Bradley, A. and Caskey, C.T. (1994) Hyperuricemia and urate nephropathy in urate oxidase-deficient mice. Proc. Natl. Acad. Sci. USA 91 (2), 742–746.
[22] Freitas, S., Spencer, P.J., Vassão, R.C. and Abrahão-Neto, J. (2010) Biochemical and biopharmaceutical properties of PEGylated uricase. Int. J. Pharm. 387 (1–2), 215–222.
[23] Malaguarnera, G., Giordano, M. and Malaguarnera, M. (2012) Rasburicase for the treatment of tumor lysis in hematological malignancies. Expert Rev. Hematol. 5 (1), 27–38.
[24] Pession, A., Melchionda, F. and Castellini, C. (2008) Pitfalls, prevention, and treatment of hyperuricemia during tumor lysis syndrome in the era of rasburicase (recombinant urate oxidase). Biologics 2 (1), 129–141.

Human Molecular Genetics, 2012, Vol. 21, No. 4 **765–775**
doi:10.1093/hmg/ddr508
Advance Access published on November 7, 2011

Molecular and cellular characteristics of *ABCA3* mutations associated with diffuse parenchymal lung diseases in children

Florence Flamein[1], Laure Riffault[1], Céline Muselet-Charlier[1], Julie Pernelle[1], Delphine Feldmann[3], Laurence Jonard[3], Anne-Marie Durand-Schneider[1], Aurore Coulomb[4], Michèle Maurice[1], Lawrence M. Nogee[6], Nobuya Inagaki[7], Serge Amselem[2], Jean Christophe Dubus[8], Virginie Rigourd[9], François Brémont[10], Christophe Marguet[11], Jacques Brouard[12], Jacques de Blic[13], Annick Clement[1,5], Ralph Epaud[14,15] and Loïc Guillot[1,*]

[1]Inserm U938 and [2]Inserm U933, UPMC, Univ Paris 6, France, [3]Department of Biochemistry, [4]Department of Pathology and [5]Department of Pediatric Pulmonology, Reference Center for Rare Respiratory Diseases in Children, Armand Trousseau Hospital, AP-HP, Paris, France, [6]Division of Neonatology, Department of Pediatrics, Johns Hopkins University School of Medicine, Baltimore, MD, USA, [7]Department of Diabetes and Clinical Nutrition, Graduate School of Medicine, Kyoto University, Kyoto, Japan, [8]Department of Pediatrics, Timone University Hospital, Marseille, France, [9]Institut de Puériculture de Paris, Paris, France, [10]Department of Pediatric Pulmonology and Allergology, Centre Hospitalo-Universitaire (CHU), Toulouse, France, [11]Department of Pediatric Pulmonology and Allergology, CHU, Charles Nicolle, Rouen, France, [12]Department of Pediatrics, CHU de Caen, Caen, France, [13]Department of Pediatric Pulmonology-Allergology, Université Paris Descartes, Hôpital Necker Enfants Malades, AP-HP, Paris, France, [14]Inserm U955, Créteil, France and [15]Université Paris Est, Créteil, France

Received August 29, 2011; Revised and Accepted October 29, 2011

ABCA3 (ATP-binding cassette subfamily A, member 3) is expressed in the lamellar bodies of alveolar type II cells and is crucial to pulmonary surfactant storage and homeostasis. *ABCA3* gene mutations have been associated with neonatal respiratory distress (NRD) and pediatric interstitial lung disease (ILD). The objective of this study was to look for *ABCA3* gene mutations in patients with severe NRD and/or ILD. The 30 *ABCA3* coding exons were screened in 47 patients with severe NRD and/or ILD. *ABCA3* mutations were identified in 10 out of 47 patients, including 2 homozygous, 5 compound heterozygous and 3 heterozygous patients. SP-B and SP-C expression patterns varied across patients. Among patients with *ABCA3* mutations, five died shortly after birth and five developed ILD (including one without NRD). Functional studies of p.D253H and p.T1173R mutations revealed that p.D253H and p.T1173R induced abnormal lamellar bodies. Additionally, p.T1173R increased IL-8 secretion *in vitro*. In conclusion, we identified new *ABCA3* mutations in patients with life-threatening NRD and/or ILD. Two mutations associated with ILD acted via different pathophysiological mechanisms despite similar clinical phenotypes.

INTRODUCTION

Pulmonary surfactant, a complex mixture of lipids and specific proteins located at the air–liquid interface, lowers alveolar surface tension, thereby preventing alveolar collapse at the end of expiration. It is synthesized by alveolar type-II cells, stored in lamellar bodies and secreted by exocytosis. Phospholipids make up ~90% of pulmonary surfactant.

Recent studies indicate a role for several genes in diffuse lung diseases (1–3). Genes implicated to date include the

*To whom correspondence should be addressed at: INSERM U938, Bâtiment Kourilsky, 184 rue du Faubourg Saint Antoine, 75012 Paris, France. Tel: +33 149284682; Fax: +33 143401748; Email: loic.guillot@inserm.fr

Table 1. Genetic analysis results in the 10 children harboring homozygous and compound heterozygous (shaded) or heterozygous *ABCA3* mutations

Patient	NRD	Clinical outcome	*ABCA3* mutation cDNA level	Protein level	*ABCA3* SNPs dbSNPs rs# cluster id	*ABCA3* variants Missense variants in conserved amino acid
1	Yes	ILD	c.[3518C>G] + [3518C>G]	p.[T1173R] + [T1173R]	rs149532, rs13332514	
2	Yes	ILD	c.[757G>C] + [757G>C]	p.[D253H] + [D253H]		
3	Yes	Death	c.[1385T>G] + [2890G>A]	p.[L462R] + [G964S]	rs149532	
4	Yes	Death	c.[4747C>T] + c.[384delC]	p.[R1583W] + p.[S128Rfs]	rs149532	c.[450G>A] (het)
5	No	Death	c.[629G>T] + [3079G>C]	p.[G210V] + [A1027P]	rs149532	
6	Yes	ILD	c.[622C>T] + [4561C>T]	p.[R208W] + [R1521W]	rs149532, rs323043	
7	Yes	Death	c.[604G>C] + [907C>G]	p.[G202R] + [L303V]	rs149532, rs323043 (het), rs13332514	
8	Yes	Death	c.[2888A>G] + [?]	p.[Y963C] + [?]	rs149532 (het), rs323043 (het)	
9	Yes	ILD	c.[2125C>T] + [?]	p.[R709W] + [?]	rs149532	
10	Yes	ILD	c.[2614A>G] + [?]	p.[S872G] + [?]	rs149532 (het), rs323043, rs13332514 (het)	

het, heterozygous; NRD, neonatal respiratory distress; ILD, interstitial lung disease.

surfactant protein (SP)-B and SP-C genes (*SFTPB*, MIM 178640; and *SFTPC*, MIM 178620) and the ATP-binding cassette subfamily A member 3 gene (*ABCA3*, MIM 601615). SP-B deficiency has long been known to cause lethal neonatal respiratory distress (NRD) (4). More recently, *SFTPC* mutations were reported in newborns and infants with severe alveolar-interstitial syndrome (3,5). ABCA3 is a 1704-amino acid protein expressed selectively—but not specifically—in the lung, where it is found in the limiting membrane of lamellar bodies (1,6,7). ABCA3 is encoded by an 80 kb gene mapped to 16p13.3 in humans and is thought to regulate lipid transport and organization during lamellar body formation (8,9).

ABCA3 gene mutations are transmitted by autosomal recessive inheritance. As with SP-B deficiency, ABCA3 deficiency should be suspected in full-term infants with severe NRD refractory to maximal conventional treatment (10,11). In addition, *ABCA3* gene mutations have been found in children and young adults with interstitial lung disease (ILD) (1,3,12). For instance, the heterozygous c.875A>T (p.Glu292Val, p.E292V) *ABCA3* mutation was identified in several older children and young adults with desquamative interstitial pneumonitis (1). The large size and marked allelic heterogeneity of the *ABCA3* gene create challenges in mutation identification.

The objectives of this study were to identify and characterize *ABCA3* variations in a large population of pediatric patients with NRD and/or ILD. We identified new *ABCA3* gene mutations and found that these mutations were not associated with a specific expression profile of SP-B and SP-C in bronchoalveolar lavage fluid (BALF). Functional analysis of two mutations associated with ILD showed different pathophysiological mechanisms, despite the similar clinical phenotype.

RESULTS

Study patients

Of the 47 children enrolled in the study (Supplementary Material, Supporting Information 1), 23 (49%) were male and 24 (51%) female. The patients were from Europe ($n = 27$), North Africa ($n = 12$), Reunion Island ($n = 6$), West Africa ($n = 1$) and Haiti ($n = 1$). Among them, 6 (13%) were born prematurely (<36 weeks) and 31 (66%) had NRD. ILD developed in 31 (66%) patients, and 21 (36%) patients had both NRD and ILD. Nine (19%) patients died of respiratory failure.

Genetic analysis

Of the 47 patients, 10 had *ABCA3* mutations. We identified 15 mutations, including 13 that had not been described previously. The two mutations p.G210V and p.R208W have been already identified (13,14). There were 14 missense mutations and 1 heterozygous nonsense mutation (p.Ser128ArgfsX23, designated hereafter as p.S128Rfs) (Table 1).

Analysis of genomic DNA from the parents and kindred showed that the compound heterozygous p.R1583W/p.S128Rfs (Fig. 1A) and p.R208W/p.R1521W (Fig. 1B) mutations were inherited, as well as the homozygous mutations p.T1173R (Fig. 1C) and p.D253H (Fig. 1D). For the other mutations, genomic DNA samples from family members were not available.

None of these newly identified *ABCA3* mutations has been previously described as polymorphisms (http://ncbi.nih.gov/SNP). In addition, none of the new variants was detected in the 46 alleles from our 23 controls. Alignment of the human and other mammalian amino acid sequences (by Multiple Sequence Comparison using Log-Expectation, MUSCLE analysis) indicated that almost all the *ABCA3* mutations occurred in highly conserved residues (not illustrated). They were located across the protein in the extracellular domains (ECD1 and ECD2), as well as in internal domains (NBD1 and NBD2) (Fig. 2). Finally, complete *ABCA3* sequencing disclosed previously described single-nucleotide polymorphisms (SNPs) (Table 1), as well as a missense variant affecting a conserved amino acid in the patient harboring the c.[4747C>T]+[384delC] mutation.

In the 37 patients without *ABCA3* mutations, four SNPs were identified in the coding region of *ABCA3*. These SNPs were in exons 7, 9, 14 and 26, respectively, and did not induce amino acid variations. A missense variant in the conserved amino acid c.1059C>T was identified in nine children. We found these variants neither in the public polymorphism database nor in our controls.

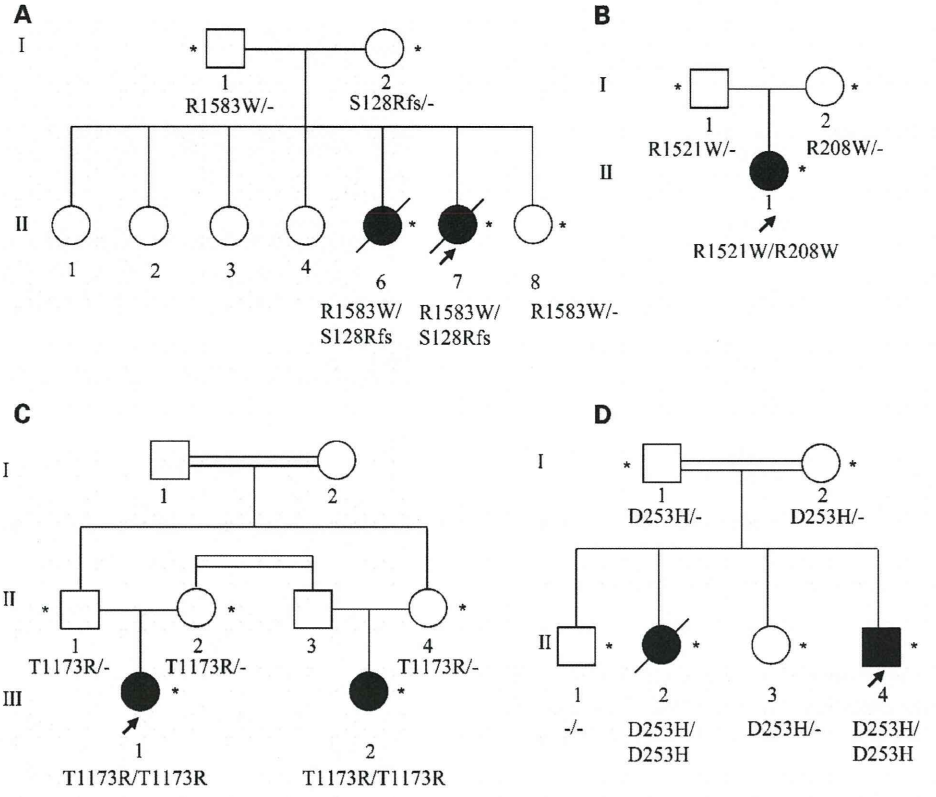

Figure 1. Pedigree of the families with the *ABCA3* mutations p.R1583W/p.S128Rfs (**A**), p.R1521W/R208W (**B**), p.T1173R/p.T1173R (**C**) and p.D253H/p.T1173R (**D**). Asterisks indicate family members with ABCA3 mutation analysis, and arrows indicate index patients.

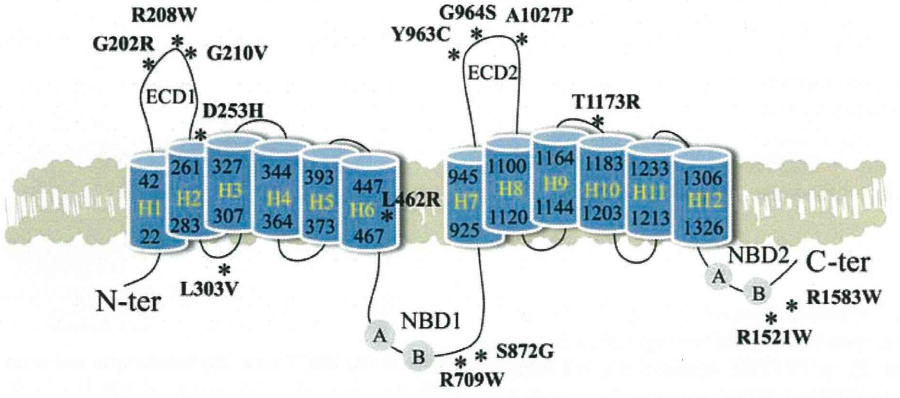

Figure 2. Schematic representation of the ABCA3 protein [N-terminal (N-ter) to C-terminal (C-ter) domains] and the location of the novel mutations (indicated by an asterisk). The 12 putative transmembrane helix (H1–H12) domains, two extracellular domains (ECD1 and ECD2) and two nucleotide-binding domains (NBD) (including the conserved motifs Walker A and B) are represented.

Characteristics of patients with *ABCA3* mutations

The characteristics of the 10 children with ABCA3 mutations are reported in Table 2. Among them, nine (90%) had NRD, five progressed to ILD and five died of respiratory failure (all during the first year of life).

Three children harboring homozygous and compound heterozygous mutations who developed ILD (patients 1, 2 and 6) were treated with methylprednisolone pulse for, respectively, 14 months (patient 1), 6 years (patient 2) and 11 years (patient 6, who is still on methylprednisolone pulse). They also received azithromycin for, respectively, 2 years (patient 1), 12 years (patient 2) and 2 years (patient 6), patients 2 and 6 still being treated. Two patients (patients 2 and 6) required prolonged oxygen supplementation for, respectively, 10 years (patient 2) and 11 years (patient 6, who is still on oxygen).

Two children harboring heterozygous mutations developed ILD (patients 10 and 9). The first child (patient 10) was

Table 2. Clinical characteristics of the 10 patients with *ABCA3* mutations

	ABCA3-mutated patients ($n = 10$)
Sex: male/female, *n* (%)	4 (40)/6 (60)
Median age at onset in months (range)	0 (0–6)
Neonatal respiratory distress, *n* (%)	9 (90)
Hypoxemia, *n* (%)	10 (100)
Physical findings, *n* (%)	
Tachypnea	10 (100)
Retractions	10 (100)
HRCT findings, *n* (%)	
Ground-glass opacities	8 (100)
Lung cysts	3 (38)
Interlobular septal thickening	2 (25)
Consolidation	4 (50)
Lung biopsy, *n* (%)	
Type-II cell hyperplasia	6 (100)
Septal thickening	6 (100)
Mild fibrosis	5 (83)
Intra-alveolar macrophages	6 (100)
Outcome *n* (%)	
ILD/death	5 (50)/5 (50)

ILD, interstitial lung disease; *n* corresponds to the number of available patients' clinical data.

treated by monthly methylprednisolone pulse for 3 years and required oxygen supplementation for 8 months. The second one (patient 9) did not receive any treatment during the study period.

All 10 patients had clinical symptoms of respiratory failure. High-resolution computed tomography (HRCT) scans were available for eight patients and predominantly showed ground-glass opacities (Fig. 3A and Supplementary Material, Supporting Information 2). Lung biopsy was performed in six patients, all of whom had alveolar septal thickening, a few interstitial inflammatory cells (polymorphonuclear neutrophils and lymphocytes), uniform prominent type-II cell hyperplasia and accumulation of intra-alveolar macrophages (Fig. 3B). Electron microscopy was performed on a lung biopsy from the patient harboring the p.D253H mutation and showed abnormal lamellar bodies with dense inclusions (Fig. 3C).

BALF analysis

Western blot analysis of surfactant proteins (Fig. 4) was performed in seven patients, who had the following *ABCA3* mutations: p.D253H (patient 2), p.T1173R (patient 1), p.L462R/p.G964S (patient 3), p.G202R/p.L303V (patient 7), p.Y963C (patient 8), p.R1583W/p.S128Rfs (patient 4) and p.S872G (patient 10), respectively. SP-C (Fig. 4A) and SP-B (Fig. 4B) were detected at a size of 3.7 and 8 kDa in variable amounts, the smallest amount being found in the patient with the p.G202R/p.L303V *ABCA3* mutation (patient 7) in whom SP-C and SP-B are only faintly visible. This patient was the only one who cannot be weaned off mechanical ventilation before he died of respiratory failure. Interestingly, the two children harboring homozygous mutations (patients 1 and 2) have small but detectable amounts, which were nonetheless compatible with life. In contrast, patient 4, who died within the first month of life, had amount of SP-B and SP-C similar to control.

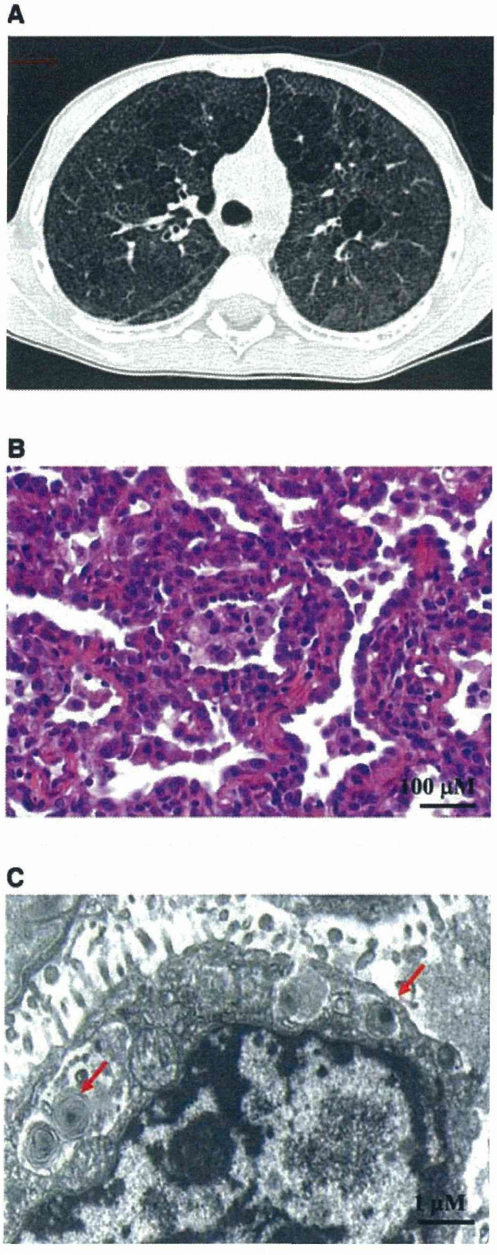

Figure 3. (**A**) HRCT scan, (**B**) hematoxylin and eosin (HE) staining of lung tissue and (**C**) electron microscopy of type-II cells from the patient (patient 2) harboring the *ABCA3* homozygous mutation p.D253H. Red arrows indicate lamellar bodies.

Characterization of ABCA3 mutations

The two mutations p.T1173R and p.D253H were deliberately chosen for subsequent functional studies because they were homozygous. Also, since past functional studies of ABCA3 focused mainly on NRD-associated mutations, it was crucial to study the consequences of these two mutations associated with progression towards ILD.

ABCA3 localization and processing. We first investigated the intracellular localization of the mutated ABCA3 protein.

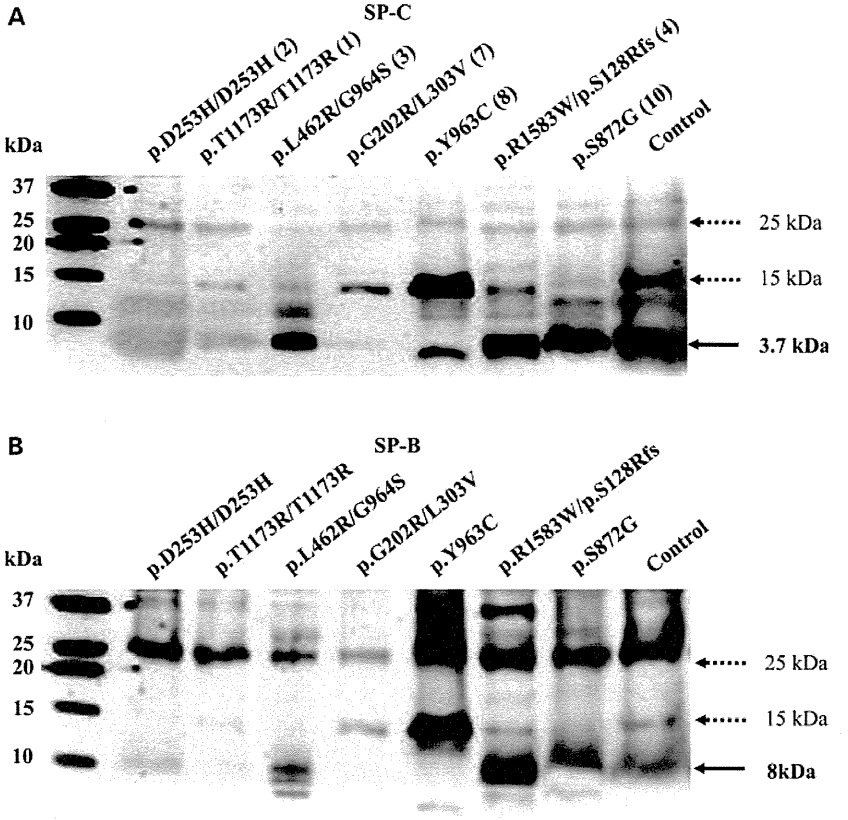

Figure 4. Western blot analysis of surfactant proteins B and C (SP-B and SP-C, respectively) in BALF from seven patients with *ABCA3* mutations and from a control without ILD. Dashed arrows indicate proSP-C (15 and 25 kDa) and proSP-B (15 and 25 kDa). Plain arrows indicate mature SP-C (3.7 kDa) and SP-B (8 kDa).

Similar to the WT protein, ABCA3 mutants co-localized with Lysotracker staining and partially with ERtracker staining (Fig. 5). ABCA3 might co-localize with ER during their folding. However, no accumulation in the ER was observed. The same results were obtained with transiently transfected cells (data not shown). Thus, p.D253H and p.T1173R mutants were not associated with a localization defect. ABCA3 expression was studied on protein extracts from A549-transfected cells. In WT, p.T1173R and p.D253H cells, anti-GFP antibody revealed two bands of 180 kDa (150 kDa ABCA3 + 30 kDa GFP) and 220 kDa (190 + 30 kDa GFP), respectively (Fig. 6). As previously suggested, these two bands might reflect two processing forms (15–18).

Lamellar bodies in ABCA3 WT, p.D253H and p.T1173R cells. Lamellar bodies were not observed in A549 cells (Fig. 7). As shown previously with HEK293 cells (15), transfection of ABCA3 in A549 cells is sufficient to induce lamellar body formation (Fig. 7). The p.D253H mutation induced abnormal lamellar bodies with electron-dense inclusions (Fig. 7, dashed arrows), consistent with the results of the patient's lung biopsy (Fig. 3C). In cells transfected with the p.T1173R mutation, abnormal lamellar bodies are the most frequently observed (irregularly arranged, phospholipid lamellae but eccentrically packed), even if some appeared almost normal.

Cytokine production by ABCA3 WT, p.D253H and p.T1173R cells. We next investigated whether ABCA3 mutants could induce inflammation. IL-8 was chosen as a well-known marker in inflammatory chronic lung disease. Using quantitative PCR (qPCR), we found that IL-8 mRNA levels were increased in p.T1173R cells (Fig. 8A). A significant, faint increase in IL-8 mRNA expression was also observed between WT and p.D253H cells. ABCA3 mRNA levels were similar in WT and mutated cells (data not shown), indicating that the increased IL-8 mRNA level in p.T1173R cells was not due to a transfection issue. At the protein level, ELISA results confirmed that A549 cells expressing the p.T1173R mutant produced more IL-8 than did WT cells (Fig. 8A). In contrast, IL-8 production by p.D253H cells was similar to that of WT cells (Fig. 8B). Finally, TGF-β and MCP-1secretions were similar between WT and transfected cells (data not shown).

IL-8 production is controlled chiefly by MAPK and NF-κB signaling (19). To determine whether these signaling pathways were involved in the observed IL-8 overproduction by p.T1173R cells, we used specific inhibitors. Treatment of cells with inhibitors of MAPK (p38, JNK, ERK1/2) and NF-κB showed that IL-8 production (in WT and mutant cells) was mainly ERK1/2 dependent. The lack of involvement of NF-κB was confirmed by measuring NF-κB promoter activity as done previously (20) (data not shown). However, with

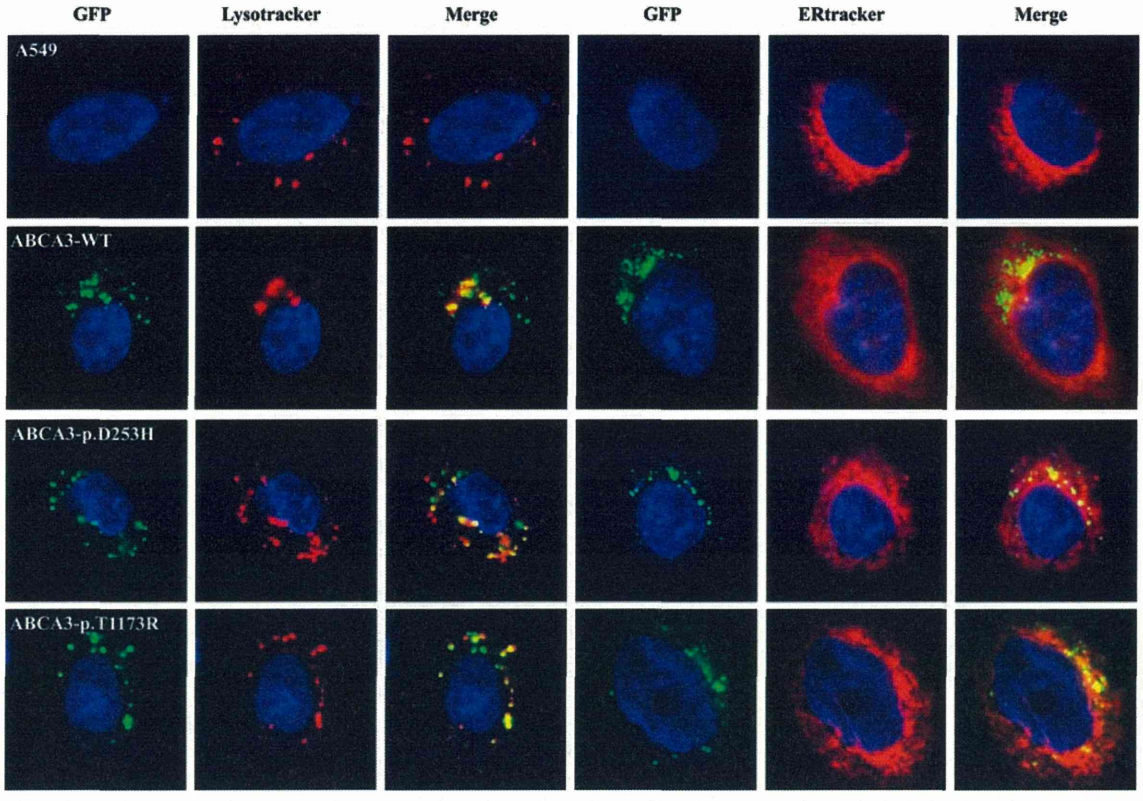

Figure 5. Intracellular localization of wild-type ABCA3 and of the p.D253H and p.T1173R mutants. A549 cells either non-transfected or transfected with mock vector, wild-type protein ABCA3-WT (**A**) or mutated proteins p.D253H (**B**) and p.T1173R (**C**) were analyzed using confocal microscopy. Lysotracker and ERtracker were used to stain lysosomes and the endoplasmic reticulum, respectively.

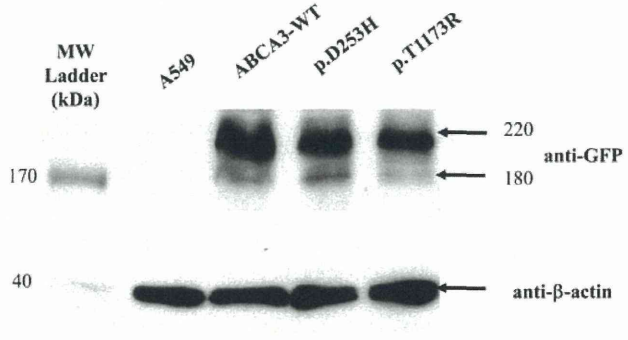

Figure 6. Western blot analysis of ABCA3 in cells transiently transfected with ABCA3-WT or the p.D253H or p.T1173R mutation. ABCA3 expression was detected using anti-GFP antibody (top panel). Equal loading was verified using anti-β actin antibody (bottom panel).

ERK1/2 inhibitor treatment, IL-8 production by p.T1173R cells remained increased compared with WT and p.D253H cells. These results suggest that, even if ERK1/2 signaling is involved in IL-8 production, another signaling pathway may be involved in the increased IL-8 production detected in p.T1173R cells.

Western blot and relative quantification of ERK1/2 phosphorylation confirmed that the observed IL-8 overproduction in p.T1173R cells was independent of ERK1/2 signaling. Finally, caspase 3/7 activity was similar in WT and mutant cells, indicating that these mutations did not induce apoptosis.

DISCUSSION

We identified 15 (13 novel) *ABCA3* mutations in 47 children (32%) who had NRD and/or ILD and no *SFTPB* or *SFTPC* mutations (5). None of these mutations was found in either the public polymorphism database or our controls. The amino acids affected by the mutations were conserved in mammalian *ABCA3* sequences. All 10 patients with *ABCA3* (21%) mutations had severe respiratory symptoms and abnormal chest imaging findings. Ninety percent of patients harboring *ABCA3* mutations had NRD. Finally, parents heterozygous for the p.R1583W, p.S128Rfs, p.R1521W or p.R208V mutations were not affected. In three patients, a mutation was found in a single allele but the clinical phenotype (NRD) may support the existence of a second mutation (in introns, deletions and so on) not detected by our sequencing method. Haploinsufficiency has been suggested as a mechanism leading to clinical phenotype emergence in patients with only one mutated allele (10,21). Similarly, *Abca3*$^{+/-}$ mice, despite normal respiratory function, had fewer lamellar bodies and altered surfactant lipid synthesis compared with wild-type mice, suggesting susceptibility to NRD or ILD (22). However, even if the observed clinical phenotypes are

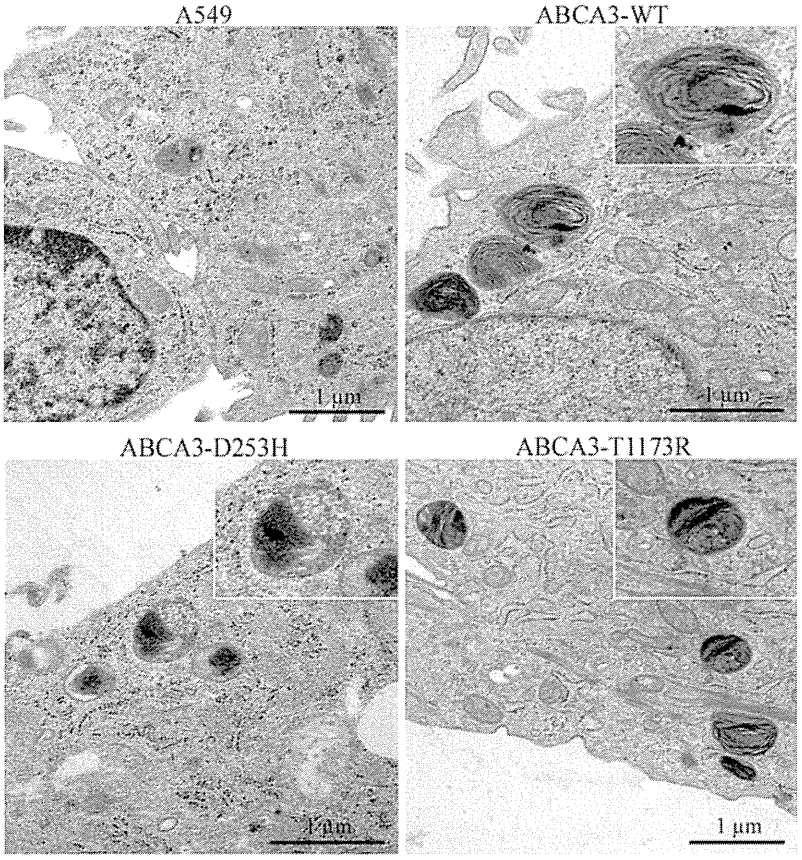

Figure 7. Lamellar body analysis. A549 cells transfected with mock vector (pEGFP-N1), ABCA3-WT (**A**), or mutated ABCA3-D253H (**B**) or ABCA3-T1173R-GFP were analyzed using electron microscopy.

compatible with *ABCA3* deficiency, we cannot conclude that *ABCA3* heterozygosis is responsible for this phenotype.

As previously described (1,11,13), some patients with *ABCA3* mutations had a less severe phenotype than that usually associated with *ABCA3* mutations (10). These variations in the clinical and radiological features may be related to the nature of the mutation (16). Previous studies showed that *ABCA3* mutations led to abnormal processing and/or trafficking of the ABCA3 protein (15), alterations in ABCA3 protein functions such as ATPase activity (16), or impaired lipid transport (23). Interactions with variants in other genes and/or with external factors such as viral infections may also influence the observed phenotype (24).

ABCA3 deficiency in full-term patients with NRD was shown previously to be associated with abnormal processing of SP-B and SP-C with an accumulation of precursors of SP-B and absence of mature SP-C (11). In our patients with *ABCA3* deficiency, we observed that SP-C and SP-B expression levels varied considerably across patients. Indeed, less severe patients had decreased amounts of SP-B and SP-C, whereas patient who died of respiratory failure showed normal expression of both proteins. This discrepancy may be explained by our technique of western blot, which is performed on lyophilized supernatant and improved the level of surfactant protein detection. It may also be explained by the function of ABCA3, which is critical for the proper formation of lamellar bodies and surfactant function but is not responsible for SP-B or SP-C synthesis. Hence, the pattern of SPs may be independent of the clinical status. To confirm the hypothesis, it would have been interesting to compare the patterns of siblings harboring the p.D253H mutation. Unfortunately, BALF from this patient was not available. Finally, as reported previously for *SFTPC* mutations (25), the presence or absence of SP-B and SP-C might be neither sensitive nor specific for *ABCA3*-related diseases.

Electron microscopy examination of a lung biopsy specimen is the reference standard for evaluating lamellar body characteristics and for providing a preliminary diagnosis prior to *ABCA3* gene analysis. Indeed, abnormal lamellar bodies with electron-dense inclusions have been described in association with *ABCA3* mutations in previous studies (10,21,26). However, electron microscopy cannot be performed routinely. The presence of abnormal lamellar bodies in the patient harboring the p.D253H mutation supports a pathogenic effect of this mutation. These abnormalities were also observed *in vitro* in p.D253H- and p.T1173R-transfected cells, suggesting that *ABCA3* abnormalities may consistently induce abnormal lamellar bodies. However, since we do not have the corresponding biopsy from the patient harboring the p.T1173R, we cannot draw a firm conclusion on this point.

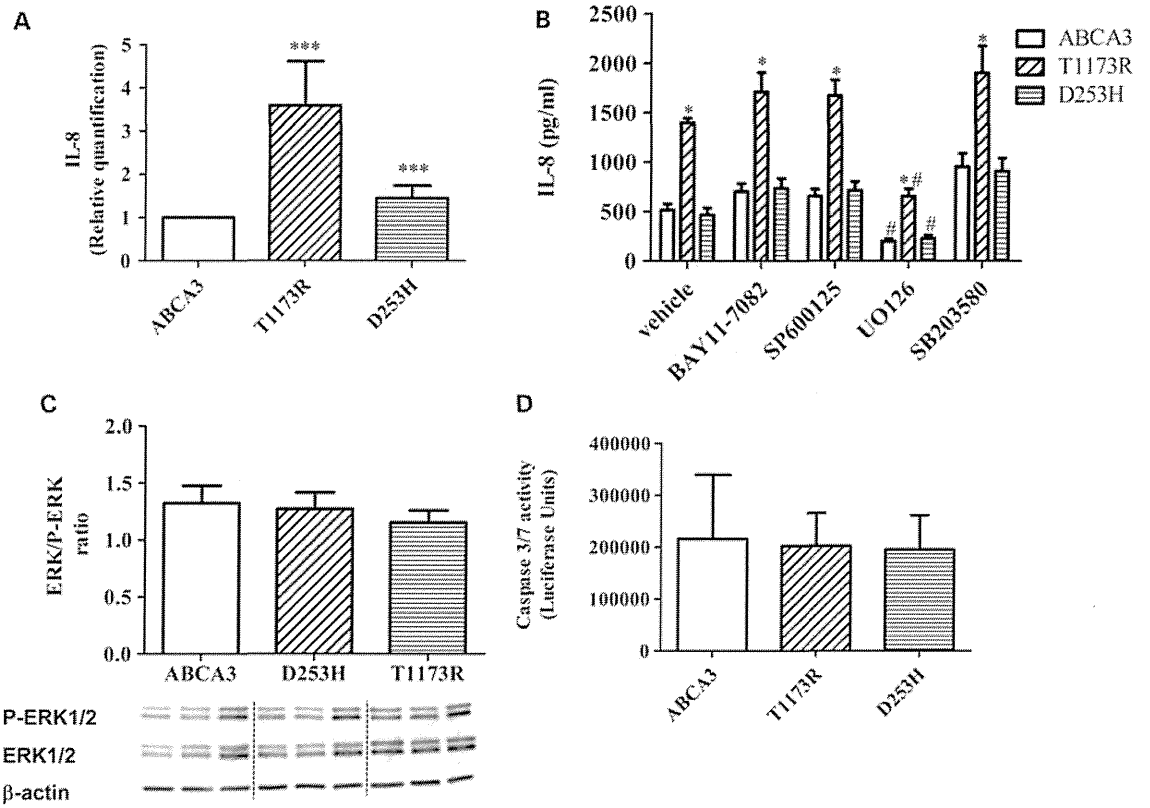

Figure 8. (**A**) IL-8 mRNA relative quantification was performed using qPCR. Results are representative of the mean ± SD of three experiments performed in triplicate. $^{***}P \leq 0.001$. (**B**) Role for MAPK and NF-κB-dependent signaling in IL-8 secretion by ABCA3-WT, D253H and T1173R cells. Cells were treated with 10 μM inhibitors of ERK1/2 (U0126), p38 (SB203580), JNK (SP600125) or NF-κB (BAY11-7082) for 24 h; $^{*}P \leq 0.05$: ABCA3 versus T1173R; $\#P \leq 0.05$: vehicle versus U0126. Supernatants were tested for IL-8 by ELISA. Data are means ± SD of three experiments performed in triplicate. (**C**) ERK1/2 phosphorylation measurement. Data are means ± SD of four experiments performed in triplicate. Results are expressed as P-ERK/ERK ratio (top panel). Western blot analysis of phospho-ERK1/2, total ERK1/2 and β-actin (bottom panel). (**D**) Caspase 3/7 activity. Data are means ± SD of three experiments performed in triplicate.

We performed *in vitro* experiments to elucidate the pathophysiological effects of two mutations associated with progression towards ILD, p.D253H and T1173R. These mutations did not alter the localization or maturation of the protein. Past functional studies on other *ABCA3* mutations showed localization/folding defects or functional defects (15,16,18,21,23,27). As pointed out recently, the effect of *ABCA3* mutations on lung epithelial cells depends on the ABCA3 protein defects (18). We found that the functional abnormalities differed between the two mutations. The p.D253H and p.T1173R mutations induced abnormal lamellar bodies. ABCA3 being a major transporter of phosphatidylcholine and phosphatidylglycerol into lamellar bodies, the lamellar body alterations suggest abnormalities in phospholipid trafficking that need to be characterized. The recent proteomic characterization of lamellar bodies may help to achieve this challenging objective (28). The p.T1173R mutation was also associated with increased production of IL-8, a well-known chemotactic molecule for neutrophils. Interestingly, increased IL-8 production was also detected in cells expressing *SFTPC* (Δexon 4 and the common p.I73T) mutations (29). In contrast, we do not find differences in TGF-β production, a cytokine that has been extensively studied in adults with idiopathic pulmonary fibrosis (30). Also, no differences in MCP-1 production were observed between WT and mutated cells. MCP-1 has been shown previously to contribute to the pathogenesis of pediatric ILD (31). However, in this study, none of the children had familial ILD, and surfactant genetic screening was not done, thus we do not know whether MCP-1 production is related to surfactant-associated disorders. In fact, surfactant genetic disorders are a subclass of pediatric ILD (2), which include various clinical phenotypes associated with specific clinical and biological features. Altered intercellular signaling was also shown recently in cells expressing *SFTPC* variants. CXCR1 and CCR2 expression by lymphocytes and neutrophils is probably dependent on an unidentified soluble mediator secreted by p.I73T cells (32). These studies, combined with our data, suggest that inflammatory pathways are involved in genetic surfactant disorders. However, better characterization of these pathways is required if specific treatments are to be sought.

In conclusion, although rare, ABCA3 deficiency should be considered in full-term newborns with severe respiratory distress and in older patients with ILD. Since *ABCA3* mutations lead to distinct functional defects, functional analysis of each *ABCA3* mutation is necessary to identify specific molecular targets that could be modulated or corrected by therapeutic agents.

MATERIALS AND METHODS

Patients

Through a national program on rare lung diseases, which has been described elsewhere (5), we recruited 121 pediatric patients with diffuse lung disease, over a 5-year period (2002–2007). Among the 121 patients with diffuse lung disease, 86 had respiratory distress, 59 presenting with neonatal onset (NRD) and 18 patients died. *ABCA3* genetic screening was performed in 47 children with severe respiratory distress or familial history compatible with autosomal recessive inheritance. Patients with presence of *SFTPC* or *SFTPB* mutations or insufficient information from medical records were excluded.

For each patient, we retrieved the following information from the medical records: family history, clinical presentation, findings by radiography and HRCT of the chest and lung biopsy findings (including those obtained by electron microscopy). The control for the BALF study was one child with uveitis who underwent bronchoscopy because of suspected sarcoidosis. Bronchoscopy showed no evidence of sarcoidosis or ILD. The control population for the genetic tests consisted of 23 individuals of European descent who had no history of lung disease. The protocol was accepted by the appropriate Committee for the Protection of Individuals in Biochemical Research, as required by French legislation. Written informed consent was obtained from the patients or their next of kin before study inclusion (5).

Genetic analysis

Genomic DNA was extracted from blood samples using an automated BioRobot EZ1 workstation (Qiagen, Hilden, Germany). Parental DNA was sequenced when samples were available. *ABCA3* primers were designed to amplify the 30 coding exons and their respective splice junctions (10). Primers were purchased from Sigma-Aldrich (Lyon, France) and Taq polymerase from Applied Biosystems (Foster City, CA, USA). Sequencing reactions were performed as described previously (5). Identified mutations were verified on two PCR products. Nucleotide numbering reflected *ABCA3* cDNA numbering, with +1 corresponding to the A of the ATG translation initiation codon in the reference sequence NM_001089.2. The reference sequence NP_001080.2 of ABCA3 protein was used for amino acid numbering.

Histological examination of lung tissue

Lung tissue obtained by surgical biopsy was examined by light microscopy using a standard hematoxylin and eosin staining protocol. Electron microscopy was conducted using standard protocols.

Collection of BALF

We retrospectively analyzed BALF from seven children with *ABCA3* mutations. Fiber-optic bronchoscopy with bronchoalveolar lavage was performed under sedation, as previously described (33).

ABCA3 vectors

The pEGFPN1-ABCA3 plasmid, called ABCA3-WT hereafter, was obtained as described previously (16). Mutagenesis was induced using PCR-based site-directed mutagenesis (QuikChange Site-Directed Mutagenesis Kit, Stratagene, La Jolla, CA, USA). Mutagenesis primers (Sigma) were as follows: *D253H-For*-5′-ACCCGCCGTTCATCGCACACCCCTTCC-3′, *D253H-Rev*-5′-GGAAGGGGTGTGCGATGAACGGCGGGT-3′; *T1173R-For*-5′-ACGTGCGTGCCTTCAGGCGGGACG-3′, and *T1173R-Rev*-5′-CGTCCCGCCTGAAGGCACGCACGT-3′. Mutagenesis was confirmed by sequencing.

Cell culture and transfection

A549 cells were cultured as described previously (34). Cells (1×10^6) were transfected with 1 μg of ABCA3-WT, ABCA3-D253H or ABCA3-T1173R plasmid using a nucleofector device (Lonza, Cologne, Germany) as recommended by the manufacturer. For stable transfection, GFP-positive cells were selected using a FACSAria cell sorter (BD, Le Pont-De-Claix, France) and plated with 0.5 mg/ml of Geneticin (Invitrogen, Paisley, UK). Three weeks after selection, stably transfected cells were examined by immunofluorescence and maintained with 0.3 mg/ml of Geneticin. Experiments with transiently transfected cells (Lipofectamine, Invitrogen) were performed 24 h post-transfection. Analysis of NF-κB activation was done with NF-κB luciferase plasmid (20).

Fluorescence microscopy

Cells transfected transiently or stably with A549 were plated in 35 mm Petri dishes (iBidi, Martinsried, Germany). Living cells were stained with either Lysotracker red (lysosome probe) or ERtracker red (endoplasmic reticulum probe) (Invitrogen, Paisley, UK). DAPI (Sigma-Aldrich, Lyon, France) was used to stain the nucleus. Fluorescence microscopy was achieved using a Zeiss Axiovert 200 microscope (Zeiss, Le Pecq, France).

Cytokine/ERK ELISA and caspase 3/7

Cells stably transfected with A549 (1×10^5) were seeded in 96-well plates (TPP, Trasadingen, Switzerland). After 24 h, the cells were incubated with vehicle (DMSO) or 10 μM inhibitors of ERK1/2 (U0126), p38 (SB203580), JNK (SP600125) (Sigma-Aldrich) or NF-κB (BAY11-7082) (Calbiochem, San Diego, CA, USA). Human IL-8, MCP-1 and TGF-β concentrations in cell culture supernatants were determined 24 h later using the DuoSet enzyme-linked immunosorbent assay kit (R&D Systems, Minneapolis, MN, USA). Relative ERK1/2 phosphorylation was measured using a cell-based ERK1/2 ELISA kit (RayBiotech, Norcross, GA, USA) following the manufacturer's instructions. Caspase 3/7 activity (Promega, Madison, WI, USA) was measured as recommended by the manufacturer.

IL8 real-time qPCR

Total RNA was extracted using a nucleospin extract II kit (Macherey Nagel, Duren, Germany). Reverse transcription was performed with 0.8 μg of total extracted RNA, using the ABI high-capacity cDNA archive kit (Applied Biosystems). RT-PCR was performed using an ABI StepOnePlus™. Each reaction contained 10 μl of 2× TaqMan® Fast Universal PCR Master Mix (Applied Biosystems), 1 μl of IL-8 (Hs00174103_m1), ABCA3 (Hs00975518_m1) or GAPDH (Hs03929097_g1) TaqMan® probe and 40 ng of cDNA as the template in a final volume of 20 μl. Data were analyzed using the comparative C_t method ($\Delta\Delta C_t$). For relative quantification, the amount of IL-8 was normalized for GAPDH (endogenous gene) relative to wild-type cells (ABCA3-WT) used as the calibrator and was calculated using the $2^{-\Delta\Delta C_t}$ method as published previously (35). Each point corresponds to the mean ± SD of three experiments performed in triplicate.

Western blot

BALF proteins were accurately quantified using a Qubit fluorometer (Invitrogen). Then, 24 μg of protein was fractionated using SDS–PAGE on 16% Tris–tricine gels, electrotransferred and probed by immunoblotting using antibodies to surfactant proteins SP-B and SP-C (Seven Hills Bioreagents, Cincinnati, OH, USA), as described previously (33).

A549 cell extracts were prepared from 3×10^5 cells and solubilized as described previously (34). An equal amount of protein (10 μg) from each sample was size-separated on 10% SDS–polyacrylamide gel and electrotransferred to a nitrocellulose membrane (Bio-Rad, Hercules, CA, USA). Immunodetection was performed with antibodies specific for the total and phosphorylated forms of ERK1/2 (Cell Signaling Technology, Beverly, MA, USA) and β-actin (Sigma-Aldrich). Secondary antibodies were from Cell Signaling Technology. Bound antibodies were detected using Super-Signal West Femto chemiluminescent substrate (Pierce, Rockford, IL, USA) according to the manufacturer's instructions. Between successive probes, membranes were treated with Restore Western Blot Stripping Reagent (Pierce). Molecular masses were determined using the SeeBlue® Plus2 Pre-Stained Standard (Invitrogen). Images were recorded with a Fujifilm LAS-3000 bioimaging system (Fujifilm, Stamford, CT, USA).

For the study of ABCA3 expression, 35 μg of transiently transfected cells (Lipofectamin, 48 h) was used. Immunoblotting was performed with an anti-eGFP antibody (Clontech, Mountain View, CA, USA).

Statistics

The statistical significance of differences between groups was tested using the unpaired Student's *t*-test with a threshold of $P < 0.05$.

SUPPLEMENTARY MATERIAL

Supplementary Material is available at *HMG* online.

ACKNOWLEDGEMENTS

We thank the patients and their families for their cooperation in this study. We are grateful to Marie-Claude Miesch, Catherine Meunier, France Michel, Corinne Chauve, Isabelle Sargis and Magali Niasme for their expert technical assistance. We thank Professor M. Griese and Dr R. Zarbock for assistance with ABCA3 western blotting. We thank A. Wolfe for assistance in improving the manuscript.

Conflict of Interest statement. None declared.

FUNDING

This work was supported by a Legs Poix (Chancelleries des Universités de Paris, to L.G.), the Assistance Publique-Hôpitaux de Paris [Surfactant Disorders and Chronic Lung Disease (APSE), ClinicalTrials.gov #NCT00783978, to R.E.] and from the United States National Institutes of Health (HL54703 to L.M.N.). F.F. was supported by a PhD fellowship from the SPLF (Société de Pneumologie de Langue Française).

REFERENCES

1. Bullard, J.E., Wert, S.E., Whitsett, J.A., Dean, M. and Nogee, L.M. (2005) ABCA3 mutations associated with pediatric interstitial lung disease. *Am. J. Respir. Crit. Care. Med.*, **172**, 1026–1031.
2. Deutsch, G.H., Young, L.R., Deterding, R.R., Fan, L.L., Dell, S.D., Bean, J.A., Brody, A.S., Nogee, L.M., Trapnell, B.C., Langston, C. *et al.* (2007) Diffuse lung disease in young children: application of a novel classification scheme. *Am. J. Respir. Crit. Care. Med.*, **176**, 1120–1128.
3. Hartl, D. and Griese, M. (2005) Interstitial lung disease in children—genetic background and associated phenotypes. *Respir. Res.*, **6**, 32.
4. Nogee, L.M., Garnier, G., Dietz, H.C., Singer, L., Murphy, A.M., deMello, D.E. and Colten, H.R. (1994) A mutation in the surfactant protein B gene responsible for fatal neonatal respiratory disease in multiple kindreds. *J. Clin. Invest.*, **93**, 1860–1863.
5. Guillot, L., Epaud, R., Thouvenin, G., Jonard, L., Mohsni, A., Couderc, R., Counil, F., de Blic, J., Taam, R.A., Le Bourgeois, M. *et al.* (2009) New surfactant protein C gene mutations associated with diffuse lung disease. *J. Med. Genet.*, **46**, 490–494.
6. Stahlman, M.T., Besnard, V., Wert, S.E., Weaver, T.E., Dingle, S., Xu, Y., von Zychlin, K., Olson, S.J. and Whitsett, J.A. (2007) Expression of ABCA3 in developing lung and other tissues. *J. Histochem. Cytochem.*, **55**, 71–83.
7. Mulugeta, S., Gray, J.M., Notarfrancesco, K.L., Gonzales, L.W., Koval, M., Feinstein, S.I., Ballard, P.L., Fisher, A.B. and Shuman, H. (2002) Identification of LBM180, a lamellar body limiting membrane protein of alveolar type II cells, as the ABC transporter protein ABCA3. *J. Biol. Chem.*, **277**, 22147–22155.
8. Connors, T.D., Van Raay, T.J., Petry, L.R., Klinger, K.W., Landes, G.M. and Burn, T.C. (1997) The cloning of a human ABC gene (ABC3) mapping to chromosome 16p13.3. *Genomics*, **39**, 231–234.
9. Klugbauer, N. and Hofmann, F. (1996) Primary structure of a novel ABC transporter with a chromosomal localization on the band encoding the multidrug resistance-associated protein. *FEBS Lett.*, **391**, 61–65.
10. Shulenin, S., Nogee, L.M., Annilo, T., Wert, S.E., Whitsett, J.A. and Dean, M. (2004) ABCA3 gene mutations in newborns with fatal surfactant deficiency. *N. Engl. J. Med.*, **350**, 1296–1303.
11. Brasch, F., Schimanski, S., Muhlfeld, C., Barlage, S., Langmann, T., Aslanidis, C., Boettcher, A., Dada, A., Schroten, H., Mildenberger, E. *et al.* (2006) Alteration of the pulmonary surfactant system in full-term infants with hereditary ABCA3 deficiency. *Am. J. Respir. Crit. Care. Med.*, **174**, 571–580.
12. Whitsett, J.A., Wert, S.E. and Xu, Y. (2005) Genetic disorders of surfactant homeostasis. *Biol. Neonate.*, **87**, 283–287.
13. Doan, M.L., Guillerman, R.P., Dishop, M.K., Nogee, L.M., Langston, C., Mallory, G.B., Sockrider, M.M. and Fan, L.L. (2008) Clinical,

radiological and pathological features of ABCA3 mutations in children. *Thorax*, **63**, 366–373.
14. Somaschini, M., Nogee, L.M., Sassi, I., Danhaive, O., Presi, S., Boldrini, R., Montrasio, C., Ferrari, M., Wert, S.E. and Carrera, P. (2007) Unexplained neonatal respiratory distress due to congenital surfactant deficiency. *J. Pediatr.*, **150**, 649–653, 653 e641.
15. Cheong, N., Madesh, M., Gonzales, L.W., Zhao, M., Yu, K., Ballard, P.L. and Shuman, H. (2006) Functional and trafficking defects in ATP binding cassette A3 mutants associated with respiratory distress syndrome. *J. Biol. Chem.*, **281**, 9791–9800.
16. Matsumura, Y., Ban, N., Ueda, K. and Inagaki, N. (2006) Characterization and classification of ATP-binding cassette transporter ABCA3 mutants in fatal surfactant deficiency. *J. Biol. Chem.*, **281**, 34503–34514.
17. Nagata, K., Yamamoto, A., Ban, N., Tanaka, A.R., Matsuo, M., Kioka, N., Inagaki, N. and Ueda, K. (2004) Human ABCA3, a product of a responsible gene for abca3 for fatal surfactant deficiency in newborns, exhibits unique ATP hydrolysis activity and generates intracellular multilamellar vesicles. *Biochem. Biophys. Res. Commun.*, **324**, 262–268.
18. Weichert, N., Kaltenborn, E., Hector, A., Woischnik, M., Schams, A., Holzinger, A., Kern, S. and Griese, M. (2011) Some ABCA3 mutations elevate ER stress and initiate apoptosis of lung epithelial cells. *Respir. Res.*, **12**, 4.
19. Hoffmann, E., Dittrich-Breiholz, O., Holtmann, H. and Kracht, M. (2002) Multiple control of interleukin-8 gene expression. *J. Leukoc. Biol.*, **72**, 847–855.
20. Muselet-Charlier, C., Roque, T., Boncoeur, E., Chadelat, K., Clement, A., Jacquot, J. and Tabary, O. (2007) Enhanced IL-1beta-induced IL-8 production in cystic fibrosis lung epithelial cells is dependent of both mitogen-activated protein kinases and NF-kappaB signaling. *Biochem. Biophys. Res. Commun.*, **357**, 402–407.
21. Park, S.K., Amos, L., Rao, A., Quasney, M.W., Matsumura, Y., Inagaki, N. and Dahmer, M.K. (2010) Identification and characterization of a novel ABCA3 mutation. *Physiol. Genomics*, **40**, 94–99.
22. Cheong, N., Zhang, H., Madesh, M., Zhao, M., Yu, K., Dodia, C., Fisher, A.B., Savani, R.C. and Shuman, H. (2007) ABCA3 is critical for lamellar body biogenesis in vivo. *J. Biol. Chem.*, **282**, 23811–23817.
23. Matsumura, Y., Ban, N. and Inagaki, N. (2008) Aberrant catalytic cycle and impaired lipid transport into intracellular vesicles in ABCA3 mutants associated with nonfatal pediatric interstitial lung disease. *Am. J. Physiol. Lung Cell. Mol. Physiol.*, **295**, L698–707.
24. Bullard, J.E. and Nogee, L.M. (2007) Heterozygosity for ABCA3 mutations modifies the severity of lung disease associated with a surfactant protein C gene (SFTPC) mutation. *Pediatr. Res.*, **62**, 176–179.
25. Hamvas, A. (2006) Inherited surfactant protein-B deficiency and surfactant protein-C associated disease: clinical features and evaluation. *Semin. Perinatol.*, **30**, 316–326.
26. Edwards, V., Cutz, E., Viero, S., Moore, A.M. and Nogee, L. (2005) Ultrastructure of lamellar bodies in congenital surfactant deficiency. *Ultrastruct. Pathol.*, **29**, 503–509.
27. Matsumura, Y., Sakai, H., Sasaki, M., Ban, N. and Inagaki, N. (2007) ABCA3-mediated choline-phospholipids uptake into intracellular vesicles in A549 cells. *FEBS Lett.*, **581**, 3139–3144.
28. Ridsdale, R., Na, C.L., Xu, Y., Greis, K.D. and Weaver, T. (2010) Comparative proteomic analysis of lung lamellar bodies and lysosome-related organelles. *PLoS One*, **6**, e16482.
29. Maguire, J.A., Mulugeta, S. and Beers, M.F. (2011) Endoplasmic reticulum stress induced by surfactant protein C BRICHOS mutants promotes proinflammatory signaling by epithelial cells. *Am. J. Respir. Cell Mol. Biol.*, **44**, 404–414.
30. Willis, B.C. and Borok, Z. (2007) TGF-beta-induced EMT: mechanisms and implications for fibrotic lung disease. *Am. J. Physiol. Lung Cell. Mol. Physiol.*, **293**, L525–534.
31. Hartl, D., Griese, M., Nicolai, T., Zissel, G., Prell, C., Reinhardt, D., Schendel, D.J. and Krauss-Etschmann, S. (2005) A role for MCP-1/CCR2 in interstitial lung disease in children. *Respir. Res.*, **6**, 93.
32. Woischnik, M., Sparr, C., Kern, S., Thurm, T., Hector, A., Hartl, D., Liebisch, G., Mulugeta, S., Beers, M.F., Schmitz, G. *et al.* (2010) A non-BRICHOS surfactant protein c mutation disrupts epithelial cell function and intercellular signaling. *BMC Cell Biol.*, **11**, 88.
33. Guillot, L., Carre, A., Szinnai, G., Castanet, M., Tron, E., Jaubert, F., Broutin, I., Counil, F., Feldmann, D., Clement, A. *et al.* (2010) NKX2-1 mutations leading to surfactant protein promoter dysregulation cause interstitial lung disease in 'brain-lung-thyroid syndrome'. *Hum. Mutat.*, **31**, E1146–E1162.
34. Guillot, L., Medjane, S., Le-Barillec, K., Balloy, V., Danel, C., Chignard, M. and Si-Tahar, M. (2004) Response of human pulmonary epithelial cells to lipopolysaccharide involves Toll-like receptor 4 (TLR4)-dependent signaling pathways: evidence for an intracellular compartmentalization of TLR4. *J. Biol. Chem.*, **279**, 2712–2718.
35. Guillot, L., Carroll, S.F., Badawy, M. and Qureshi, S.T. (2008) Cryptococcus neoformans induces IL-8 secretion and CXCL1 expression by human bronchial epithelial cells. *Respir. Res.*, **9**, 9.